Development of Fluidized Catalytic Reactors: Screening and Scale-Up

Vaibhav V. Kelkar and Ka M. Ng
Dept. of Chemical Engineering, University of Massachusetts, Amherst, MA 01003

A systematic procedure that helps develop gas-solid and gas-liquid-solid catalytic fluidized-bed reactors has two components—screening and scale-up. In screening, a reactor type is selected first from the variety of multiphase reactors. If fluidized-bed reactors are chosen, further screening is carried out using experimentally verified models to account for the detailed hydrodynamic features of the reactor. Decisions are made on the fluidization regime, heat management scheme, solid recirculation, use of reactor internals, and so on. In addition, heuristics are presented to anticipate and address issues such as catalyst agglomeration, breakage and deactivation, and changes in the nature of fluidization over the long term. The second component provides criteria to directly scale up the bench reactor to the production reactor, while maintaining a selected reactor performance index such as conversion, product yield, and selectivity.

Introduction

Fluidized beds have been used in many catalytic, as well as noncatalytic, chemical processes. Examples include the oxidation of naphthalene to phthalic anhydride, propylene ammoxidation to acrylonitrile, hydrogenation of nitrobenzene to aniline, Fischer Tropsche synthesis, and various kinds of fermentation processes. Fluidized-bed reactors, which can be operated in a variety of fluidization modes and configurations as shown in Figure 1, are particularly attractive for reactions that are highly exothermic or with rapidly deactivating catalysts. There exists an extensive literature on fluidization and fluidized-bed reactors, including several notable texts and monographs (Davidson and Harrison, 1971; Grace, 1982; Yates, 1983; Fan, 1989; Kunii and Levenspiel, 1991; Kwauk, 1994).

In a typical reactor development project, the proposed reaction is first investigated by the chemist in a microreactor or a bench-scale reactor (Ihara et al., 1996). At this stage, despite the uncertainty regarding reaction kinetics, and potential limitations of heat and mass transfer, it is critical that the best reactor type—not necessarily a fluidized bed—be identified. Kelkar and Ng (1998, 2000) developed a systematic procedure for screening a wide variety of multiphase reactors at this early stage of process development. However, the current procedure is not sufficiently refined to capture the complex hydrodynamics in fluidized-bed reactors.

Irrespective of how decisions are made, if a fluidized bed is selected, such a candidate reactor is further developed through scale-up, along with modeling and simulations. Bergougnou et al. (1986) discussed bubble size control, grid design, entrainment and particle recovery systems, among other aspects. Jazayeri (1995) proposed a step-by-step scale-up program from the laboratory to the production reactor, and addressed design issues such as those related to catalyst particle size, degree of backmixing, and the effect of internals in the bed. Matsen (1996) highlighted various difficulties in fluidized-bed scale-up, caused by gas bypassing, solids backmixing, and malfunctions in solids flow due to particle agglomeration, and so on.

Focusing on hydrodynamics, Matsen and Tarmy (1970) and Zenz (1982) discussed scale-up criteria for fluidized beds in the slugging regime. Glicksman and coworkers (Glicksman, 1984; Glicksman et al., 1993), and Horio and coworkers (1986, 1989) approached the problem from a more fundamental viewpoint; scale-up criteria were developed to maintain hydrodynamic similarity in bubbling beds. None of these, however, considered the presence of kinetic or mass-transfer effects.

Correspondence concerning this article should be addressed to K. M. Ng at this current address: Dept. of Chemical Engineering, Hong Kong University of Science and Technology, Clear Water Bay, Hong Kong.
Current address of V. V. Kelkar: M C Research and Innovation Ctr., 444 Castro St., Suite 505, Mountain View, CA 94041.

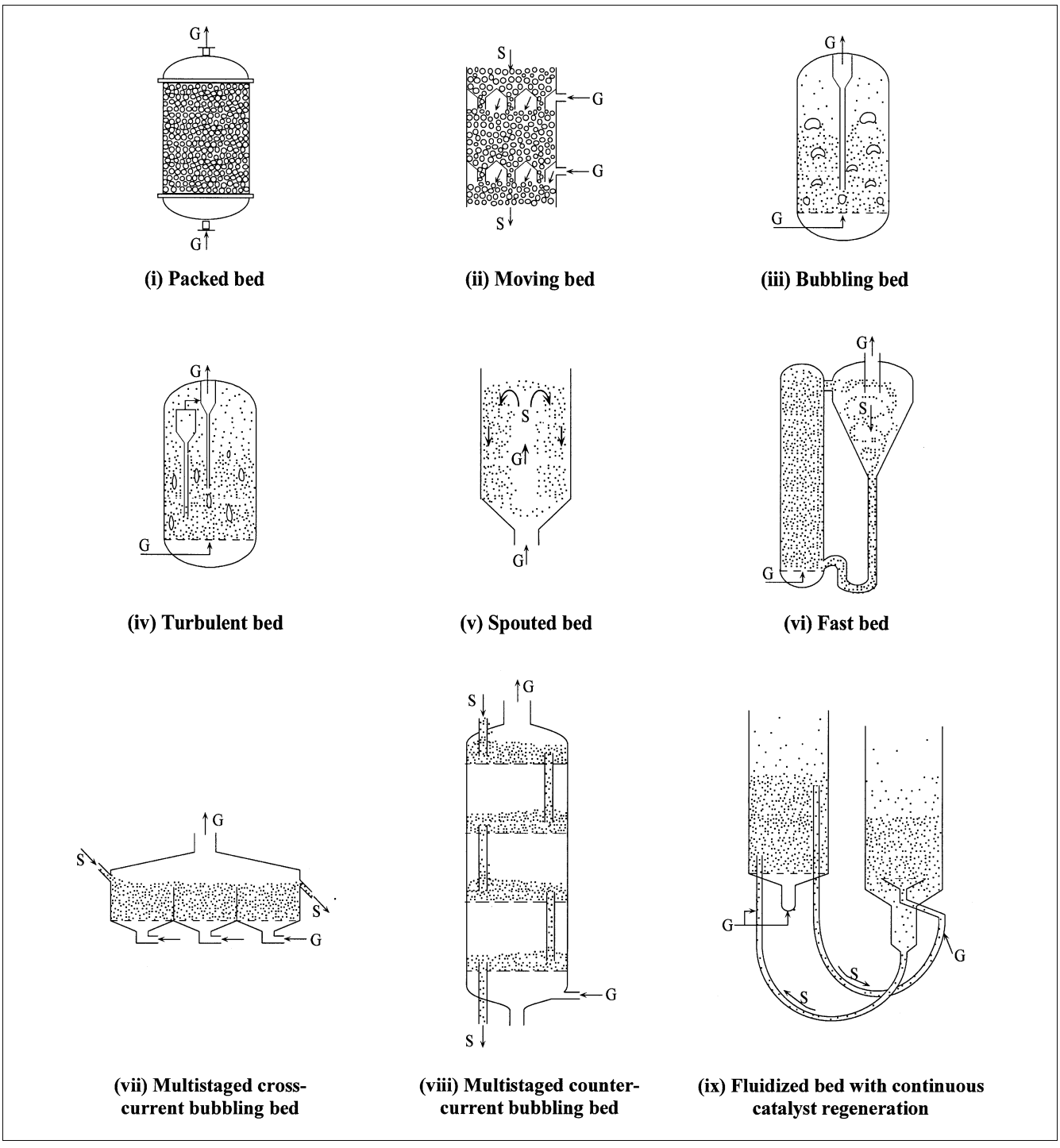

Figure 1. Selected gas-solid catalytic fluidized-bed reactors.

This study has two objectives: screening and scale-up. The screening procedure of Kelkar and Ng is expanded and refined for fluidized-bed reactors. Experimentally verified models are used to more accurately represent the complex hydrodynamic features of the reactor (Grace, 1971, 1984; Horio and Wen, 1977; Fane and Wen, 1982; Yates, 1983; van Swaaij, 1985; Chen and Too, 1986). For example, the division and exchange of gas between phases for reactors operating in various configurations and flow regimes can be accounted for. In addition, heuristics and quantitative measures are used to tackle issues such as catalyst agglomeration, breakage, deactivation, and change in fluidization behavior over the long term, which are not easily amenable to modeling. The second objective is to provide criteria to directly scale up the bench reactor to the production reactor, while maintaining a selected reactor performance index such as conversion, product

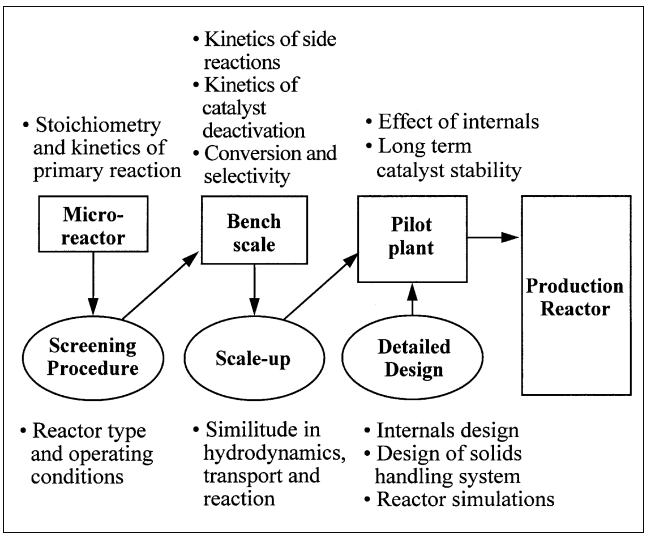

Figure 2. Development procedure for fluidized catalytic reactors.

yield, or selectivity. This is demonstrated for gas-solid catalytic reactors operating in the bubbling regime.

Figure 2 shows how these screening and scale-up methods (in ovals) fit into a typical development program. The objectives of each step in reactor development are also enumerated. We focus on gas-solid and gas-liquid-solid catalytic fluidized-bed reactors in this study.

Screening

Conventional multiphase reactors are decomposed into four building blocks: *phase distribution attributes, topological and geometrical characteristics, reactor constituent parts, and transport and thermodynamic parameters*. Basic information of reaction kinetics and physicochemical properties of the system forms the input to the screening procedure. The three elements to the screening step include a hierarchy of reactor models, an accompanying sensitivity model, and a knowledge base consisting of heuristics and correlations on hydrodynamics, heat, and mass transport.

In the preliminary screening stage, the reactor models have to be sufficiently generic to represent a broad class of reactors, including packed and trickle beds, fluidized beds, and slurry reactors. The purpose of the model at this stage is not to simulate the reactors in detail, but to distinguish between different reactor types on the basis of reactor parameters, the phase distribution, macroscopic mixing patterns in all phases, and the geometry of the reactor. Network models as developed by Kelkar and Ng are used here because of their computational convenience. Once a fluidized bed is chosen for the reaction under consideration, further screening as well as scale-up is based on models which better capture the hydrodynamics in such reactors (Wen, 1984).

A few representative models for gas-solid and gas-liquid-solid fluidized-bed reactors are shown in Figures 3 and 4, respectively. Figure 3a represents a pseudo-homogeneous model. Figure 3b represents a two-phase model where the gas bubbles form one phase, and the gas-solid emulsion forms

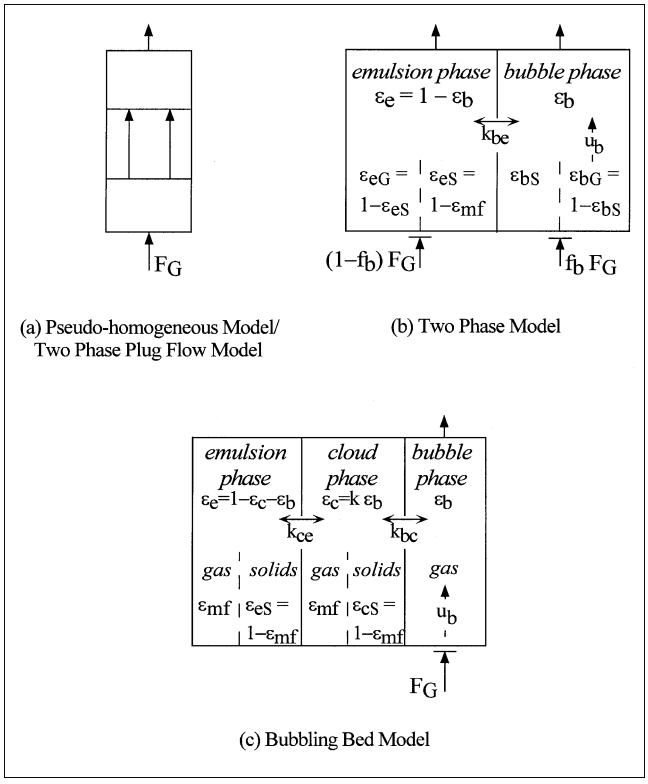

Figure 3. Selected models for gas-solid catalytic fluidized-bed reactors.

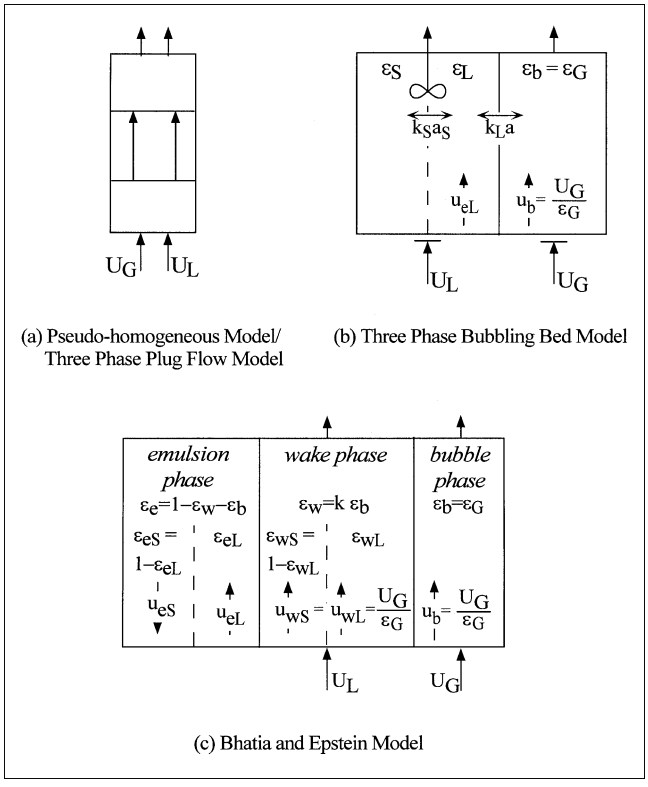

Figure 4. Selected models for gas-liquid-solid catalytic fluidized-bed reactors.

Table 1. Models for Gas-Solid Fluidized-Bed Reactors

Pseudohomogeneous Model

$$-U_G\frac{dG_A}{dz}-\epsilon_S\Phi_A=0$$
$$G_A(0)=G_A^f$$

Two-Phase Model

gas phase
$$-f_bU_G\frac{dG_A}{dz}-k_{be}a(G_A-E_A)-\epsilon_b\epsilon_{bS}\Phi_{A,b}=0$$
$$G_A(0)=G_A^f$$

emulsion phase (plug)
$$-(1-f_b)U_G\frac{dE_A}{dz}+k_{be}a(G_A-E_A)-(1-\epsilon_b)(1-\epsilon_{\mathrm{mf}})\Phi_{A,e}=0$$

(well mixed)
$$(1-f_b)F_G(G_A^f-E_A)+\int_0^H A_Tk_{be}a(G_A-E_A)dz-A_TH(1-\epsilon_b)\epsilon_{eS}\Phi_{A,e}=0$$

Bubbling Bed Model

gas phase
$$-U_G\frac{dG_A}{dz}-k_{bc}a(G_A-C_A)=0$$
$$G_A(0)=G_A^f$$

cloud phase (well mixed)
$$k_{bc}a(G_A-C_A)-k_{ce}a(C_A-E_A)-\epsilon_c\epsilon_{cS}\Phi_{A,c}=0$$

emulsion phase (well mixed)
$$k_{ce}a(C_A-E_A)-\epsilon_e\epsilon_{eS}\Phi_{A,e}=0$$

Two-Phase Plug-Flow Model

gas phase
$$-U_G\frac{dG_A}{dz}-k_Sa_S(G_A-S_A)=0$$
$$G_A(0)=G_A^f$$

solid phase
$$-U_S\frac{dS_A}{dz}+k_Sa_S(G_A-S_A)-\epsilon_S\Phi_A=0$$
$$S_A(0)=0$$

Table 2. Hydrodynamic Relations for Gas-Solid Fluidized-Bed Reactors

General

$$Ar=\frac{\rho_G(\rho_S-\rho_G)gd_p^3}{\mu_G^2}$$
$$U_{mf}=\frac{\mu_G(\sqrt{739.84-0.0408\,Ar}-27.2)}{d_p\rho_G}$$
$$D_T=\left(\frac{4wt}{\rho_S\epsilon_{S,mf}\pi(H/D_T)_{mf}}\right)^{1/3}$$
$$a=\frac{6\epsilon_b}{d_b}$$
$$u_b=0.711\sqrt{gd_b}+(U_G-U_{mf})$$
$$H=\frac{H_{mf}}{(1-\epsilon_b)}$$

Two-Phase Model

$$d_{b,\max}=1.64[A_T(U_G-U_{mf})]^{0.4}$$
$$\overline{d_b}=d_{b,\max}-(d_{b,\max}-d_{b0})e^{-0.3(H/2)D_T}$$
$$k_{be}=\frac{U_{mf}}{3}+\left(\frac{4D_e\epsilon_{mf}u_b}{\pi d_b}\right)^{1/2}$$

Bubbling Bed Model

$$k_{bc}=\frac{3}{4}U_{mf}+0.975\left(\frac{D_e^{1/2}g^{1/4}}{d_b^{1/4}}\right)$$
$$k_{ce}=\left(\frac{4D_e\epsilon_{mf}u_b}{\pi d_b}\right)^{1/2}$$
$$\epsilon_b=(U_G-U_{mf})/u_b$$

the second phase. The bubble phase carries part of the solids, thus allowing reaction to take place in the bubbles. The two-phase models of Orcutt, Davidson and Pigford (1962) and Grace (1986) can be derived as simplifying forms of this model. Figure 3c represents the three-phase bubbling bed model of Kunii and Levenspiel (1991), which considers the bubble wakes as a separate phase apart from the bubble and emulsion phases. The bubble size, which is assumed to be constant throughout the bed, is used to correlate other parameters such as the gas exchange coefficients. The selection of a particular model from the above hierarchy depends on the characteristics of the particular reacting system, as well as on the accuracy of the physicochemical data available about the reacting system.

These models are illustrated with balance equations for the gas-phase reactant A for a single solid catalyzed reaction $A \rightarrow$ products (Table 1). Starting with information about the particle size, density, total catalyst loading, and the height to diameter ratio under packed conditions, the hydrodynamic relations provided in Table 2 may be used to determine bed characteristics such as the expanded bed height, bubble diameters and velocities in the bed, the bubble to emulsion phase gas transfer coefficient, and so on.

Similarly, Figure 4a represents a pseudo-homogeneous model for a three-phase fluidized-bed reactor. A model consisting of gas bubbles, and an emulsion phase of solids and liquid is shown in Figure 4b. This is a simplified version of the well-known three-phase model by Bhatia and Epstein (1974) (Figure 4c). The three phases are the gas bubbles, the wakes which may carry some solids, and the liquid-solid fluidized emulsion phase. The balance equations for the gas-phase reactant A for a single solid catalyzed reaction $A \rightarrow$ products for all the models are given in Table 3. The relevant relationships are given in Table 4.

A sensitivity model as discussed by Kelkar and Ng accompanies the reactor model; it quantifies the impact of model parameters on the reactor performance. Based on sensitivity analysis, the appropriate attributes and constituent parts of the building blocks are aggregated to generate multiphase reactor alternatives. The decisions to be made during the screening procedure are discussed below.

Phase distribution attributes

Packed or Fluidized Solid Phase. The first major decision in synthesizing solid catalyzed reactors is whether to have the solids fixed (packed bed, trickle bed) or in motion (moving or fluidized bed). This decision is conventionally made using heuristics (Krishna and Sie, 1994), some of which are shown in Table 5. However, this can lead to conflicting decisions regarding process development. For example, consider oxidation of butane to maleic anhydride. The conventional technology for this process is based on the fixed-bed reactor. However, technologies based on the bubbling fluidized bed (BP and Alusuisse-Lummus) and the riser reactor (DuPont) are also available. Similarly, the ammoxidation of propylene to acrylonitrile can be carried out using SNAM Progetti's fixed-bed process, or the fluidized-bed process from SOHIO

Table 3. Models for Gas-Liquid-Solid Fluidized-Bed Reactors

Pseudohomogeneous Model

$$-U_G\frac{dG_A}{dz}-\epsilon_S\Phi_A=0$$

$$G_A(0)=G_A^f$$

Three-Phase Bubbling Bed Model

gas phase $$-U_G\frac{dG_A}{dz}-k_La\left(\frac{G_A}{H_A}-L_A\right)=0$$

liquid phase (mixed) $$U_L(L_A^f-L_A)+\int_0^H k_La\left(\frac{G_A}{H_A}-L_A\right)dz - Hk_Sa_S(L_A-S_A)=0$$

solid phase (mixed) $$k_Sa_S(L_A-S_A)-\epsilon_S\Phi_A=0$$

Three-Phase Plug-Flow Model

gas phase $$-U_G\frac{dG_A}{dz}-k_La\left(\frac{G_A}{H_A}-L_A\right)=0$$

liquid phase $$-U_L\frac{dL_A}{dz}+k_La\left(\frac{G_A}{H_A}-L_A\right)-k_Sa_S(L_A-S_A)=0$$

solid phase $$-U_S\frac{dS_A}{dz}+k_Sa_S(L_A-S_A)-\epsilon_S\Phi_A=0$$

Note: Equations for the Bhatia and Epstein model (Figure 4c) are not presented.

Table 4. Hydrodynamic Relations for Gas-Liquid-Solid Fluidized-Bed Reactors

General

$$Ar=\frac{\rho_L(\rho_S-\rho_L)gd_p^3}{\mu_L^2}$$

$$U_{mf,LS}=\frac{\mu_L(\sqrt{1135.69-0.0408\,Ar}-33.7)}{d_p\,\rho_L}$$

$$U_{mf}=U_{mf,LS}(1-376U_G^{0.327}\mu_L^{0.227}d_p^{0.213}(\rho_S-\rho_L)^{-0.423}$$

$$K=d_p\left(\frac{g\,\rho_L(\rho_S-\rho_L)}{\mu_L 2}\right)^{1/3}$$

$$U_t=\frac{gd_p^2(\rho_S-\rho_L)}{18\mu_L} \qquad K<2.6$$

$$=1.75\sqrt{\frac{gd_p(\rho_S-\rho_L)}{\rho_G}} \qquad K>60$$

$$Re_t=\frac{d_pU_t\,\rho_L}{\mu_L}$$

Three-Phase Bubbling Bed Model

$$n=4.65+20\frac{d_p}{D_T} \qquad Re_t<0.1$$

$$=(4.4+18d_p/D_T)Re_t^{-0.03} \qquad 0.1<Re_t<1$$

$$=(4.4+18d_p/D_T)Re_t^{-0.1} \qquad 1<Re_t<200$$

$$=4.4Re_t^{-0.1} \qquad 200<Re_t<500$$

$$=2.4 \qquad Re_t>500$$

$$\epsilon_S=(1-\epsilon_b)\left(1-\left(\frac{U_L}{U_t}\right)^{1/n}(1-\epsilon_b)^{-1/n}\right)$$

$$\epsilon_L=\left(\frac{U_L}{U_t}\right)^{1/n}(1-\epsilon_b)^{1-1/n}$$

$$H=\frac{H_{mf}\epsilon_{S,mf}}{\epsilon_S}$$

(Weissermal and Arpe, 1993). The screening procedure makes this decision systematically, by identifying the rate process dominating the overall reactor performance.

Catalyst Particle Size and Size Distribution. A proper selection of the catalyst particle-size distribution is essential to ensure good bed fluidity, small sized bubbles, good heat-transfer and gas-solid contact, and ease of solids flow. Jazayeri (1995) made suggestions regarding selection of the catalyst particle-size distribution. Although the mean particle size is selected based on the relative magnitudes of the gas-solid mass-transfer resistance and the intraparticle diffusion resistance, the particle-size distribution can be suitably modified to achieve the desired fluidization characteristics. Of course, it should be such that the operating velocity is higher than the minimum fluidization velocity of the largest particle, while the elutriation rate for the smallest particles is within acceptable limits. Some important recommendations regarding particle-size distribution selection are given below.

- Group A particles according to Geldart's classification exhibit a smooth fluidization behavior. If this is desirable, the average particle size needs to be decreased as the particle density increases, to stay in the group A behavior.
- The use of about 20–30% of fines (particles with d_p below 40 μm) improves gas-solid contact and hence leads to higher conversions. However, a higher fines content requires a good cyclone design accompanying the fluidized bed to limit particle carryover.
- Catalyst attrition is an important concern, as it causes a change in the size distribution and increases the load on the solids recovery system. Attrition tests should be carried out to ensure that the nature of fluidization is acceptable over the entire duration of a production cycle (Carson and Marinelli, 1994).

Bubbling or Bubble-Less Fluidization. This decision is important because bubbling causes extensive gas bypassing, and is unfavorable unless the gaseous reactant is present in excess. Bubbling fluidization includes the bubbling, slugging, and turbulent regimes, while bubble-less fluidization includes the fast fluidization regime, also referred to as dense phase riser transport, and dilute phase riser transport. The important characteristics of the above fluidization regimes are described in Table 6. Phase distribution and transport parameters such as the phase holdups and the mass-transfer coefficients also vary significantly with the type of fluidization regime. The typical ranges of selected parameters observed in different regimes for gas-solid and gas-liquid-solid fluidized beds are given in Tables 7 and 8, respectively.

Level of Backmixing of Gas and Solid Catalyst. The acceptable level of axial dispersion depends on the reaction system under consideration (Jazayeri, 1995). For example, the isomerization reaction in fluid-catalytic reforming is adversely affected by backmixing of reactants and catalyst, whereas the fluid-catalytic cracking reactions are such that the reaction yield is not significantly affected by backmixing. Thus, the appropriate fluidization regimes for the above reaction systems may be the transport regime and the bubbling regime, respectively. An analysis of the reaction scheme in the screening procedure identifies the acceptable level of backmixing. For generic models such as tanks in series models or

Table 5. Heuristics for Selecting between a Packed and Fluidized Mode of Operation

- If the characteristic time for catalyst deactivation is of the order of 1 year, a fixed-bed operation is preferred. If the deactivation time is of the order of 1 h, then a fluidized mode of operation is required. For intermediate cases, a swing operation involving more than one reactor may be considered.
- For highly exothermic reactions, consider fluidized mode of operation. It has much higher rates of heat transfer, and heat can be removed by circulating solid particles into and out of the reactor.
- For reaction kinetics favored by plug flow, consider a packed-bed operation, or an operation in the transport fluidization regime. For kinetics favored by mixed flow, consider bubbling fluidized-bed operation.
- For fast reactions which may face intraparticle diffusion problems, consider fluidized mode of operation, because it allows much smaller particles than a packed bed.
- For catalyst systems which are difficult to fluidize (such as titanium), or are very expensive, avoid fluidized mode of operation.
- For reactions producing nonvolatile residues in gas-solid systems (such as hydrodesulfurization of petroleum residues), avoid packed-bed operation because it may lead to plugging (choking) of the bed.
- For reaction systems in which agglomeration of catalyst particles is likely to occur (such as due to wax condensation in Fischer Tropsche synthesis), avoid fluidized-bed operation.

Table 6. Characteristics of Different Modes of Gas-Solid Fluidization

(1) *Bubbling Bed (Figure 1iii).*
- High gas-solid interfacial area.
- Considerable back-mixing in the emulsion phase, leading to a uniform temperature in the bed.
- Considerable bypassing of gas through the bubble phase.
- Low gas velocity and hence gas treating capacity.

(2) *Turbulent Fluidization (Figure 1iv).*
- Good gas-solid contact.
- Lower gas back-mixing but higher solids mixing than in bubbling beds.

(3) *Fast Fluidization (or Dense Phase Transport) (Figure 1vi).*
- Continuous entrainment of solids from the bed. By adjusting the rate of solid recirculation into the bed, a high solids concentration in the bed can be achieved. Higher throughputs possible.
- Lower back-mixing, and better gas-solid contact than in bubbling and turbulent beds.
- Suitable for cohesive or sticky materials.
- Dust control may be a problem.
- For coarse particles, transport of solids may be a problem.

(4) *Dilute Phase Transport*
- Flow of gas as well as solids is close to plug flow.
- Low solids concentration in the bed, and hence a lower reaction rate per unit bed volume. Suitable for fast reactions, or low conversions.
- May exhibit temperature gradient along reactor length.

(5) *Spouted Beds (Figure 1v)*
- Suitable for coarse particles ($d_p > 1$ mm), and sticky materials, for which it offers much better gas-solid contact than in conventional fluidized beds.
- Spout is useful in breaking up clusters of sticky particles, and the ash formed on solids.
- Offers lower pressure drop than packed beds.
- Limitations on gas throughput and particle sizes which can be handled.

the axially dispersed flow model, the degree of backmixing can be adjusted using appropriate parameters: the number of tanks in the former, and the dispersion coefficient in the latter.

Reactor constituent parts

These include bubble-emulsion interface generating devices such as gas distributors and various types of baffles which break the bubbles into smaller sizes; devices to enhance gas or solid circulation (such as draft tubes), or devices to limit circulation and backmixing of solids and gas (such as horizontal baffles which divide the reactor into stages); devices for heat management such as horizontal and vertical tubes; devices used to control or improve fluidization behavior such as vibrating or stirring equipment, or high velocity jet attritors to improve fluidization of cohesive particles; and devices forming part of the solids recovery and recirculation system such as cyclones, diplegs, nozzles, internals placed above the bed surface to limit particle carryover, and so on. Of course, a particular internal may serve more than one of the above purposes simultaneously. For example, immersed horizontal and vertical heat-transfer tubes may be designed to simultaneously act as bubble stabilizers. Harrison and Grace (1971) reviewed the characteristics of various types of tubes and baffles commonly found in fluidized-bed reactors. Papa and Zenz (1995) provided a simplified equation to design structured reactor internals in the fluidized-bed reactor to achieve close-to-plug flow.

Topological and geometrical characteristics

These include information about the overall shape and geometry of the reactor, such as the bed aspect ratio, the manner of contacting the phases, and so on. For freely bubbling beds, a higher aspect ratio usually implies larger bubble sizes, higher gas bypassing, and hence a lower gas-phase conversion. However, even for beds with internals where the bubble size can be controlled, very shallow beds ($H/D_T < 1$) can lead to excessive gas bypassing. The contacting patterns for gas-solid fluidized beds include: batch solids with gas being con-

Table 7. Phase Distribution Attributes and Transport Parameters for Packed- and Gas-Solid Fluidized-Bed Reactors

	Packed	Bubbling	Turbulent	Fast Beds	Dilute Transport	Spouted Beds
d_p	3–5 mm	50–250 μm	50–2,500 μm	30–500 μm	10–250 μm	usually > 1 mm
ϵ_S	0.5–0.6	0.3–0.5	0.2–0.3	0.05–0.25	0.02–0.1	—
U_G (m/s)	—	0.01–0.2	0.4–4.5	2–8	—	0.3–1.8
k_S (m/s)	0.001–0.2	0.01–0.02	—	—	—	—
U_{wall} (W/m$^2\cdot$K)	8–1,200	50–800	—	100–800		50–150

Table 8. Phase Distribution Attributes and Transport Parameters for Trickle-Bed and Gas-Liquid-Solid Fluidized-Bed Reactors

	Trickle Bed	Bubbling Fluidized Bed
d_p	3–5 mm	50–500 μm
ϵ_S	0.4–0.6	0.1–0.5
ϵ_G	0.1–0.4	0.05–0.2
ϵ_L	0.1–0.4	0.45–0.8
k_S (m/s)	2×10^{-6}–1×10^{-3}	5×10^{-6}–2.5×10^{-5}
$k_L a$ (s^{-1})	0.005–0.1	0.01–0.14
U_{wall} ($W/m^2\cdot K$)	500–2,000	1,000–4,500

tinuous (Figure 1iii), cocurrent upflow contacting (Figure 1vi), cross flow contacting with either the gas or the solids in cross flow (Figure 1vii), countercurrent or staged countercurrent contacting (Figure 1viii), and a circulating solids system (Figure 1ix). Countercurrent contacting maximizes gas conversion, while cross flow contacting with solids in multiple stages is suitable for gas-solid reactions where high solid conversion is required, and the gaseous reactant is relatively inexpensive. Also, the gas-phase pressure drop in countercurrent operation is higher than that in cross flow operation (Varma, 1975). For gas-liquid-solid fluidized beds, the available contacting modes include both upflow and downflow, co- and countercurrent contacting, with solids being charged independently or along with the liquid phase. These modes were examined in detail by Fan (1989).

After preliminary screening, reactor alternatives are further evaluated using more detailed models. The relative importance of hydrodynamic vs. kinetic effects determines which model is needed to better represent the reactor. For slow reaction rates (such as a first-order rate constant based on catalyst volume $< 1\ m^3/mol\cdot s$), the hydrodynamics has little impact on the reactor performance, and a simple pseudo-homogeneous model may be adequate. For faster reactions, two- or three-phase models may be required. Thus, for a gas-solid catalytic reactor, the high superficial velocity and the absence of bubbles in turbulent and fast fluidized beds suggests the use of a single- or a two-phase plug flow model for such reactors (Fane and Wen, 1982). The two-phase bubbling bed model (Figure 3b) appears to give a good representation of the performance of bubbling fluidized-bed reactors (Grace, 1986). For a three-phase fluidized-bed reactor, the three-phase model (Figure 4b) may be used for transport reactors where the superficial velocities are high. Bhatia and Epstein's (1974) three-phase bubbling bed model can be used to represent a three-phase fluidized bed operating in the bubbling regime.

Along with the reactor models, another component of the screening step is a knowledge base which guides the user to consider issues which may not be apparent in the bench-scale or pilot-plant reactors, but which may cause problems in the production reactor. These are the issues which arise during long-term operation of the reactor at reaction conditions. For example, Whitehead (1971) discussed problems associated with distributors in large-scale reactors. Heuristics to deal with these operational problems are given in Table 9.

Reactor screening as described above leads to a desirable reactor type, as well as the desired mode of operation and the flow regime. The next step is to scale up the reaction from bench reactor to pilot plant, and then to the production reactor, along with more rigorous simulations. A scale-up method is discussed below.

Table 9. Heuristics Related to Operational Problems in Commercial-Scale Fluidized Beds

Problems Caused by Reactor Internals

- If the gas distributor grid's hole pitch is too large, solid dead zones may form. The agglomerated solids may cause improper fluidization, lead to undesirable selectivity (if catalyst), or burn (if carbonaceous) resulting in high temperatures on the grid.
- If the pressure drop across the grid decreases, it may lead to plugging of the grid, or weeping of solids through the grid holes. These solids may burn or react leading to high temperatures near the grid, which can be damaging to the grid.
- Horizontal baffles across reactor cross-section may decrease the axial solids mixing leading to temperature gradients along the bed height, both of which may adversely affect selectivity.
- Baffles increase the overall pressure drop over the reactor length, and may also make it difficult to achieve fluidization in all stages.
- Baffles may create pockets of low solids region, which in oxidation reactors may lead to uncontrolled burning.
- In multistage units, fine solids entrained by gas may block the distributor of the next stage. Frequent cleaning may be required.
- Immersed tubes in small diameter beds may lead to slugging. Also, coolant leaking from bent or cracked tubes may interfere with the reaction chemistry.

Problems Caused by Agglomeration, Adhesion or Clustering of Solids

- The solid particles in the reactor may agglomerate in the presence of a feed liquid, such as in fluid coking and fluid bed calcining.
- Agglomeration of temperature sensitive solids may occur during shutdown when the reactor temperature is still high but the particles are not fluidized. Periodic fluidization with gas while the reactor cools will prevent this.
- Agglomerated solids may bog, causing improper fluidization, and leading to poor gas-solid contact.
- Agglomerated solids may plug valves, pipes, or grid holes in the reactor. They may form incrustations on the walls and on heat-transfer surfaces, leading to a lowering of the heat-transfer efficiency.
- Agglomerated catalysts may decrease catalytic activity, possibly changing the product distribution.

Problems Caused by Particle Breakage or Elutriation

- Attrition or particle breakage may change the size distribution of the catalyst and possibly change the fluidization behavior.
- Excessive particle carryover creates a greater load on the solids recovery system, leading to its failure.
- A tall freeboard region to allow for particle separation may cause promotion of side reactions. For example, in the thermal cracking of naphtha, ethylene and propylene may decompose in the freeboard.

Scale-Up

A large number of scale-up rules have been suggested in the literature. Glicksman (1984) identified a set of nondimensional parameters by nondimensionalizing the governing equations of motion for the fluids and the solids in a fluidized bed. Surface forces, as well as reaction and heat-transfer effects were ignored. If two beds are designed and operated to have identical values of all independent nondimensional parameters, then the dependent variables of the two beds must also be identical at every location within the bed, and *hydrodynamic similarity* is said to be achieved. More recently, Glicksman et al. (1993) proposed a simplified set of

dimensionless variables which relax some constraints on the dimensions of the small-scale reactor model, and hence allow greater flexibility in model design. The simplified set of dimensionless parameters to be held constant for hydrodynamic similarity are as follows

$$\frac{U_G^2}{gD_T}, \frac{\rho_G}{\rho_S}, \frac{U_G}{U_{mf}}, \frac{L_1}{L_2}, \frac{G_S}{\rho_S U_G}, \phi, \text{ and} \quad (1)$$

the dimensionless particle-size distribution.

In the region of low Reynolds number, where viscous forces dominate over inertial forces, the ratio of gas to solid density need not be matched, except for beds operating near the slugging regime. Horio et al. (1986) suggested a similarity rule which is valid in the viscous limit. The rule states that hydrodynamic similarity in a base model and a reactor model *m times* larger is obtained when (a) the geometrical and topological attributes of the bed, such as the bed diameter (D_T), height (H), distributor orifice diameter (P_n), orifice pitch (d_n) and so on, are changed in the same proportion, that is

$$m = \frac{D_T^l}{D_T^s} = \frac{P_n^l}{P_n^s} = \frac{d_n^l}{d_n^s} = \frac{d_b^l}{d_b^s} \quad (2)$$

where the superscript s refers to the smaller bench-scale model, and the superscript l refers to the *m times* larger production scale model; and (b) the minimum fluidization velocity U_m and the gas superficial velocity U_G scale as the square root of the scale ratio m. In other words

$$\sqrt{m} = \frac{U_{mf}^l}{U_{mf}^s} = \frac{\left(U_G - U_{mf}\right)^l}{\left(U_G - U_{mf}\right)^s} \quad (3)$$

Based on the simple hydrodynamic model given in Table 2, the similarity rule leads to the following equalities

$$\frac{\epsilon_S^l}{\epsilon_S^s} = \frac{\epsilon_b^l}{\epsilon_b^s} = 1, \quad \frac{U_G^l}{U_G^s} = \frac{u_b^l}{u_b^s} = \sqrt{m}, \quad \frac{wt^l}{wt^s} = m^3, \quad \text{and} \quad \frac{F_G^l}{F_G^s} = m^{5/2} \quad (4)$$

The above rules for hydrodynamic similarity have been validated by several studies which compared the bubble size and frequency, the amplitude of pressure fluctuations, the vertical voidage distribution, and so on. Horio et al. (1986) also examined how the gas interchange coefficient $k_{be}a$ scales with a scale change. According to the correlation by Davidson and Harrison (1963), the interchange coefficient is given by

$$k_{be}a = 4.5\frac{U_{mf}\epsilon_b}{d_b} + 5.85\frac{D^{1/2}g^{1/4}\epsilon_b}{d_b^{5/4}} \quad (5)$$

The first term in the above correlation represents the convection term and the second represents the contribution due to gas diffusion. Using the scaling relationships 1 to 4, it is seen that the convection term remains constant, whereas the diffusion term changes with a scale change. Horio defined a parameter β which represents the ratio of the diffusion term to the convection term in the correlation for $k_{be}a$

$$\beta = \frac{D^{1/2}g^{1/4}}{U_{mf}d_b^{1/4}} \quad (6)$$

For $\beta < 0.1$, the bubble-dense phase mass transfer is dominated by convection, whereas for $\beta > 10$, the contribution due to diffusion dominates. Also, β itself scales proportional to $m^{-3/4}$, that is, the relative importance of diffusion in the bubble-dense phase mass transfer decreases as the reactor size increases.

In order to understand how the gas exchange, as well as the reactor performance such as the conversion or product distribution, will change as one scales up a bench reactor to a production reactor, we will use a dimensionless reactor model, and examine how the dimensionless parameters vary with a scale change. If all the dimensionless parameters in the reactor model are kept constant with a scale change, a similarity in the reactor performance is expected. The model used here is the two-phase model with both the bubble and the emulsion phase in plug flow (Table 1). The reaction is assumed to be first order in A. The model is reproduced below in dimensionless form

$$-f_b\frac{d\overline{G}_A}{dZ} - N_m\left(\overline{G}_A - \overline{E}_A\right) - N_r\left(\frac{\epsilon_b\epsilon_{bS}}{\epsilon_S}\right)\overline{G}_A = 0 \quad (7)$$

$$-(1-f_b)\frac{d\overline{E}_A}{dZ} + N_m\left(\overline{G}_A - \overline{E}_A\right) - N_r\frac{(1-\epsilon_b)(1-\epsilon_{mf})}{\epsilon_S}\overline{E}_A = 0 \quad (8)$$

with boundary conditions: at $Z = 0$, $\overline{G}_A(0) = \overline{E}_A(0) = 1$

Here, Z is the dimensionless distance along the reactor height, and $\overline{G}_A$ and $\overline{E}_A$, are the dimensionless concentrations in the bubble and the dense phases, respectively. N_m and N_r are the dimensionless mass transfer and reaction numbers given by

$$N_m = \frac{k_{be}aH}{U_G} \quad (9)$$

$$N_r = \frac{k_v H\epsilon_s}{U_G} \quad (10)$$

Assuming that the bench-scale reactor operates at the same temperature and pressure as the production reactor, the reaction rate constant k_v is the same in both. Then, using the earlier scaling relationships, it is found that

$$N_r^l = \sqrt{m}\,N_r^s \quad (11)$$

For the dimensionless mass-transfer number N_m, we can examine two cases as was done for the gas interchange coefficient k_{be}

If $\beta < 0.1$,

$$N_m^l = N_m^s \tag{12}$$

If $\beta > 10$,

$$N_m^l = \frac{N_m^s}{m^{3/4}} \tag{13}$$

From Eqs. 11–13, it can be seen that in the production reactor, the reaction number increases by a factor of $\sqrt{m}$, whereas the mass-transfer number, at best, stays the same, and, at worst, decreases by 2 to 8 times for m going from 2 to 16. Obviously, the reactor conversion and product distribution will change as the reactor scale increases. It is interesting to examine whether a modification of scaling laws may allow a similarity in reactor performance to be maintained. For this, a suitable performance index (such as the conversion for single reactions, or the yield or the selectivity to the desired product for multiple reactions) needs to be chosen. If we consider the following simplifications to Eqs. 7 to 10—the bubbles are devoid of any solids ($\epsilon_{bS} = 0$), and the bubble phase carries most of the gas ($f_b = 1$), analytical expressions can be derived for the gas conversion, and product yield and selectivity, for common reaction schemes such as single, parallel and consecutive reactions. These are given in Table 10, and are seen to be functions of only the dimensionless reaction and mass-transfer numbers appearing in the model. For achieving similarity in a particular performance index during scale-up, the analytical expressions for the performance index for the small-scale, as well as the large-scale, reactor, are equated. Then, the appropriate scale-up criteria can be identified by taking into account the variation of various dimensionless parameters with the reactor scale. The use of more complicated models necessitates numerical solutions. This is discussed in more detail in the examples on scale-up below.

Examples

Example 1 discusses preliminary screening for a reaction scheme including catalytic and noncatalytic reactions. Example 2 illustrates the detailed screening procedure for a gas-liquid reaction catalyzed by a solid. Example 3 considers the scale-up of a single solid catalyzed reaction, where it is desired to keep the conversion of the gaseous reactant constant. Example 4 involves scale-up of a parallel reaction scheme,

Table 10. Conversion, Yield, and Selectivity Expressions for Common Reaction Schemes Using the Simplified Two-Phase Model

$A \xrightarrow{k_v} P$	$x_A = 1 - \exp\left(-\frac{N_r N_m}{N_r + N_m}\right)$
$A \begin{cases} \xrightarrow{k_{v1}} P \\ \xrightarrow{k_{v2}} X \end{cases}$	$x_A = 1 - \exp\left(-\frac{N_m(N_{r1}+N_{r2})}{N_m + N_{r1} + N_{r2}}\right)$ $y_P = \left(\frac{N_{r1}}{N_{r1}+N_{r2}}\right)\left[1 - \exp\left(-\frac{N_m(N_{r1}+N_{r2})}{N_m + N_{r1} + N_{r2}}\right)\right]$ $s_P = \left(\frac{N_{r1}}{N_{r1}+N_{r2}}\right)$
$A \xrightarrow{k_{v1}} P \xrightarrow{k_{v2}} X$	$x_A = 1 - \exp\left(-\frac{N_m N_{r1}}{N_m + N_{r1}}\right)$ $y_P = \left(\frac{N_{r1}}{N_{r1}-N_{r2}}\right)\left[\exp\left(-\frac{N_m N_{r2}}{N_m + N_{r2}}\right) - \exp\left(-\frac{N_m N_{r1}}{N_m + N_{r1}}\right)\right]$ $s_P = \left(\frac{N_{r1}}{N_{r1}-N_{r2}}\right)\frac{\exp\left(\frac{N_m^2(N_{r1}-N_{r2})}{(N_m+N_{r1})(N_m+N_{r2})}\right)-1}{\exp\left(\frac{N_m N_{r1}}{N_m+N_{r1}}\right)-1}$
$A \begin{cases} \xrightarrow{k_{v1}} P \xrightarrow{k_{v2}} X \\ \xrightarrow{k_{v3}} X \end{cases}$	$x_A = 1 - \exp\left(-\frac{N_m(N_{r1}+N_{r3})}{N_m + N_{r1} + N_{r3}}\right)$ $y_P = \left(\frac{N_{r1}}{N_{r1}-N_{r2}+N_{r3}}\right)\left[\exp\left(-\frac{N_m N_{r2}}{N_m + N_{r2}}\right) - \exp\left(-\frac{N_m(N_{r1}+N_{r3})}{N_m + N_{r1} + N_{r3}}\right)\right]$ $s_P = \left(\frac{N_{r1}}{N_{r1}-N_{r2}+N_{r3}}\right)\frac{\exp\left(\frac{N_m^2(N_{r1}-N_{r2}+N_{r3})}{(N_m+N_{r2})(N_m+N_{r1}+N_{r3})}\right)-1}{\exp\left(-\frac{N_m(N_{r1}+N_{r3})}{N_m+N_{r1}+N_{r3}}\right)-1}$

with the product yield being the desired performance index. Example 5 considers both the screening and the scale-up steps for the catalytic oxidation of o-xylene to phthalic anhydride.

Example 1: homogeneous and solid catalyzed gas-gas reactions

Consider the following multiple reaction scheme

$$A + B \xrightarrow{k_1} P \qquad \text{Rate} = k_1 AB$$

$$A + P \xrightarrow{k_2} X_1 \qquad \text{Rate} = k_2 AP$$

$$A_{(g)} + B_{(g)} \xrightarrow{k_3} X_{2(g)} \qquad \text{Rate} = k_3 A_{(g)} B_{(g)}$$

Here, the gaseous reactants A and B react on the surface of the catalyst to form the desired product P. A further reacts with P to form the undesired byproduct X_1. Also, at a high temperature, A and B can react homogeneously in the gas phase to form another undesirable byproduct X_2. All reactions are highly exothermic. The feed temperature is 500 K, while the coolant stream is available at 375 K. The reaction rate constants as functions of temperature, and the heats of reactions are given in Table 11a. The screening procedure to identify suitable reactor types for the above reaction can be described in the following steps.

Step 1: The yield of P, defined as the [amount of P formed]/[amount of B charged] is chosen as the performance index.

Step 2: Generic Model. A network of tanks in series is chosen to model the reactors (Kelkar and Ng, 1998, 2000). The heat transfer topology consists of internal, external, interstage, as well as heat transfer by circulation of solids from the reactor.

Step 3: Sensitivity Model. The parameters of interest are the gas-solid mass-transfer coefficient k_S, the particle diameter d_p, the reactor temperature T, and the number of tanks N in the model.

Step 4: Generate Base Case. A packed-bed reactor with minimal heat removal is chosen as the base case for this reaction (Table 11a). A constant gas-phase residence time of 60 s is maintained during the screening.

Step 5: Screen Parameters. The results of the screening procedure are shown in Table 11b. The performance index is shown in column 2, while the selectivity of P with respect to A is shown in column 3. The parameters k_S, d_p and the highest temperature in the reactor T_{high}, along with their sensitivity to the performance index, are shown in the remaining columns. The sensitivity $\overline{\Psi}$ is the ratio of the percentage change in performance index to the percentage change in the parameter of interest which produces it. The last column identifies the corresponding reactor type for each iteration.

For Iteration 1, the yield of P is very low ($y_P = 0.06$). This is because of the extremely high temperature within the reactor, which essentially amounts to a thermal runaway ($T_{\text{high}} =$ 1,200 K). The activation energies indicate that a temperature increase favors the undesirable reactions more than the desired reaction. The dominant sensitivity is that with respect to the reactor temperature ($\overline{\Psi}(T) = -16.9$), indicating that heat removal is the key issue. In iteration 2, we consider a turbulent fluidized mode of operation (Figure 1iv), which shows much better heat- and mass-transfer characteristics. Simultaneously, the number of tanks in the model is decreased from 10 to 1, the catalyst diameter is reduced to 250 μm, and the gas-solid mass-transfer coefficient is doubled to reflect the typical values observed in the fluidized mode of operation. A fluidized reactor with an internal heat transfer area of 15 m^2/m^3, which is on the higher side, achieves a yield of 0.53. However, due to the limited heat-transfer area available within the reactor, there is still a significant temperature rise across the reactor ($T_{\text{high}} = 629.3$ K).

Table 11. (a) Base-Case Parameters for Example 1: a Catalytic and Homogeneous Gas-Gas Reaction; (b) Sensitivity Analysis for Example 1

(a)

F_G	0.1 m^3/s	k_1			0.004 $e^{-24{,}000/RT}$ $(m^3/kg\cdot s)\cdot(m^3/mol)$
τ_G	60 s	k_2			4 $e^{-80{,}000/RT}$ $(m^3/kg\cdot s)\cdot(m^3/mol)$
ϵ_G	0.4	k_3			2×10^7 $e^{-120{,}000/RT}$ $m^3/mol\cdot s$
ϵ_S	0.6		*Feed conditions*		
k_S	1×10^{-3} m/s	G_A			100 mol/m^3
ΔH_1	-2×10^6 J/mol	G_B			80 mol/m^3
ΔH_2	-1×10^6 J/mol	T_{feed}			500 K
ΔH_3	-1×10^6 J/mol	T_{coolant}			375 K

(b)

	Yield of P	Selectivity of A to P	k_S (s^{-1})	$\overline{\Psi}$ (k_S)	d_p (μm)	$\overline{\Psi}$ (d_p)	T_{high} (K)	$\overline{\Psi}$ (T)	N	Corresponding reactor type
1	**0.06**	0.06	0.0005 ↓	0.014	3,000 ↓	−0.028	~1,200	**−16.9**	10 ↓	Packed reactor with internal heat transfer ($a_h = 1\ m^2/m^3$)
2	**0.53**	0.56	0.001	0.0031	250	−0.0015	629.3	**−3.0**	1	Fluidized reactor with internal heat transfer ($a_h = 15\ m^2/m^3$)
3	**0.73**	0.93	0.001	0.0032	250	−0.0016	512	**−0.46**	1	Fluidized reactor with 15% of solids, circulating.

A much more efficient way of managing the heat of reaction would be to use a circulating solids system. This allows much higher rates of heat transfer because of the high heat capacity of the solids. Iteration 3 therefore considers a reactor in the fluidized mode, with 15% of reactor solids being circulated continuously. This leads to an operation which is close to isothermal ($T_{high} = 512$ K). The yield of P is 0.73, with a selectivity of 0.93, both of which are a considerable improvement over that observed in the base case reactor.

Step 6: Identify Reactor Type. The above set of parameters indicate a bubbling fluidized-bed reactor with a 40% solid holdup and a high gas-solid mass-transfer coefficient, and a continuously circulating solid phase (Figure 1ix). The circulating catalyst particles may be regenerated in a separate fluidized vessel in case any catalyst deactivation takes place, and may be cooled to the feed temperature, before recycling back to the reactor.

Example 2: parallel gas-liquid reaction catalyzed by a solid

Consider a thermally neutral, solid catalyzed, parallel reaction scheme between a gaseous reactant A and a liquid reactant B as shown below

$$A + B \xrightarrow{k_1} P \qquad \text{rate} = k_1 A$$

$$A + B \xrightarrow{k_2} X \qquad \text{rate} = k_2 A$$

The kinetic information is given in Table 12a. The objective is to synthesize a three-phase catalytic reactor which maximizes the yield of desired product P.

Step 1: The yield of P, defined as the ratio [amount of P formed]/[amount of B reacted] is chosen as the performance index.

Step 2: Generic Model. A network of tanks in series is chosen to model the reactions. Depending on the number of tanks in the model and values of other parameters such as phase distribution and transport attributes, a whole class of three-phase catalytic reactors, from packed beds on the one hand, to transport reactors on the other hand, can be macroscopically represented by such a model.

Step 3: Sensitivity Model. The parameters of interest are the gas-liquid and the liquid-solid mass-transfer coefficient $k_L a$ and $k_S a_S$, respectively, the reaction rate constants, the particle diameter d_p, the catalyst effectiveness factors, the catalyst loading, and the number of tanks N in the model. Note that although the transport parameters may depend on the phase distribution parameters, they are treated as mathematically independent in the sensitivity analysis for reasons described previously (Kelkar and Ng, 1998).

Step 4: Generate Base Case. A packed-bed reactor (Figure 1i) is chosen as the base case for this reaction. The reactor screening is done based on a constant reactor volume of 0.25 m^3. The base case parameters are summarized in Table 12a.

Step 5: Screen Parameters. The results of the screening procedure are shown in Table 12b. The parameter $k_L a$ is shown in column 3. Gas-liquid mass transfer is not controlling at any stage; hence, $\overline{\Psi}$ $(k_L a)$ is not shown. Parameters $k_S a_S$, d_p, η_1, and w, along with their sensitivity to the performance index, are shown in the remaining columns. [The sensitivity to effectiveness factors is indicated indirectly by the sensitivity to the catalyst particle diameter, $\overline{\Psi}(d_p)$.] The reaction rate constants and their sensitivity coefficients are not shown for reasons of clarity. Similarly, the effectiveness factor for the undesirable reaction η_2 is higher than that for the desired reaction, and is not shown. The last column identifies the corresponding reactor type for each iteration.

For the packed reactor, the yield of P is 0.37, while the selectivity ratio of P to X is 6.37 (not shown). The desirable reaction suffers from severe diffusion limitations ($\eta_1 = 0.0046$) with the corresponding sensitivity coefficient being the highest [$\overline{\Psi}(d_p = -0.8$]. The next largest sensitivity coefficient is that with respect to the solid-liquid mass-transfer coefficient [$\overline{\Psi}(k_S a_S) = 0.61$]. The effectiveness factor, as well as the

Table 12. (a) Base-Case Parameters for Example 2: a Solid Catalyzed Gas-Liquid Parallel Reaction Scheme; (b) Sensitivity Analysis for Example 2

(a)

F_G	0.04 m^3/s	k_1	0.200 m^3/kg·s
F_L	0.001 m^3/s	k_2	0.005 m^3/kg·s
V	0.25 m^3	*Feed Conditions*	
ϵ_L	0.2	G_A	40 mol/m^3
ϵ_S	0.6	G_B	1,500 mol/m^3
k_S	5×10^{-5} m/s	G_P, G_X	0 mol/m^3
$k_L a$	0.1 s^{-1}		

(b)

	Yield of P	$k_L a$ (s^{-1})	$k_S a_S$ (s^{-1})	$\overline{\Psi}$ $(k_S a_S)$	d_p (μm)	η_1	$\overline{\Psi}$ (d_p)	w (kg/m^3)	$\overline{\Psi}$ (w)	N	Corresponding reactor type
1	**0.37**	0.1 ↓	0.06	**0.61**	3,000 ↓	0.0046	**−0.8**	1440 ↓	0.024	8 ↓	Trickle-bed reactor
2	**0.52**	0.25 ↓	0.12	0.64	50 ↓	0.25	**−0.74**	24 ↓	**0.1**	1 ↓	Stirred slurry reactor
3	**0.68**	0.15	0.72	0.17	250	0.027	−0.20	720	0.014	2	Three-phase fluidized bed

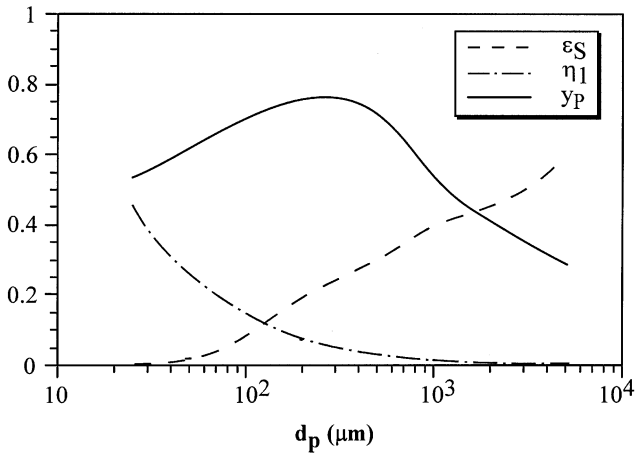

Figure 5. Dependence of reactor performance on catalyst diameter for Example 2.

mass-transfer coefficient, can be improved by decreasing the catalyst particle diameter. However, the current particle diameter of 3 mm is near the lower limit of what can be used in a packed-bed reactor, due to considerations of pressure drop. Hence, in iteration 2 we shift to a mode of operation where solids are the dispersed phase, such as in a slurry reactor. The catalyst diameter d_p is reduced to 50 μm, and the catalyst loading and the gas-liquid mass-transfer coefficient are similarly changed to reflect typical values for slurry operation. These changes are shown by downward pointing arrows in the table. Iteration 2 shows an improved yield of 0.52 and selectivity ratio of 11.8 (not shown), and a higher effectiveness factor for the desirable reaction. The dominant sensitivity coefficient is still that with respect to the particle diameter [$\overline{\Psi}(d_p) = -0.74$]. However, d_p is close to the lower limit which can be used in a slurry mode of operation. Of the other parameters, $k_S a_S$ cannot be changed independently of d_p, while $k_L a$ is close to the higher limit for slurry reactors. Therefore, the only way to increase productivity further is to increase the catalyst loading [$\overline{\Psi}(w) = 0.1$]. We note here that a fluidized mode of operation allows a much higher catalyst loading while maintaining a small particle diameter. Clearly, two opposing effects are at play here. A smaller catalyst particle diameter achieves a higher catalyst effectiveness, but also implies a lower catalyst loading. The tradeoff between the catalyst effectiveness and catalyst loading is illustrated in Figure 5 which shows the yield of P, the effectiveness factors for the desirable reaction, and the solid holdup in conventional three-phase reactors for different catalyst particle diameters. The yield of P is maximum for a catalyst diameter and a solid holdup which is typical of a fluidized mode of operation. In the third iteration we switch to a fluidized mode, with d_p and w changed suitably. The yield of P improves to 0.68, which is a considerable improvement over the base case reactor. The selectivity ratio at this stage is 6.6 (not shown).

Step 6: Identify Reactor Type. The above set of parameters indicate a three phase fluidized-bed reactor (Figure 1iii) with a solid and liquid holdup of 0.3 and 0.5 respectively, and a catalyst diameter of 1 mm. The exact flow regime of operation will be determined as described below.

As pointed out before, separate models are required to simulate the reactor performance in different fluidization regimes. The two likely regimes in three-phase fluidization are the bubbling bed regime and the riser transport regime. Since heat effects or catalyst deactivation effects are not considered in this example, the heuristics given earlier do not suggest operating in the riser transport regime. The three-phase bubbling bed model described earlier is used to simulate the bubbling bed reactor, while a plug-flow model considering the gas, liquid and solid to be separate phases is used to represent the riser reactor.

Table 13. Results for a Bubbling Fluidized-Bed Reactor (Example 2)

H	0.738 m	Yield of P	0.744
D_T	0.65 m	x_A	0.80
d_p	250 μm	P/X	7.02
U_G	0.118 m/s	G_A	7.83 mol/m^3
U_L	0.0029 m/s	L_B	224.6 mol/m^3
ϵ_S	0.4	L_P	1116.4 mol/m^3
ϵ_L	0.35	L_X	159.0 mol/m^3
k_S	5×10^{-5} m/s		
$k_L a$	0.15 s^{-1}		

For the bubbling bed reactor, a voidage of 0.55 and a height to diameter ratio of 1 is chosen at minimum fluidization conditions. A solids holdup of 0.4 is assumed in the expanded bed. The gas and liquid flow rates, the particle size, and the mass-transfer coefficients are the same as those for iteration 3 of the screening procedure. The hydrodynamic correlations given in Table 4 are used to calculate other expanded bed characteristics such as the bed height, the bubble and liquid phase holdup, and so on. The results of the evaluation are given in Table 13. The concentrations indicated in the table are those of the reactor outlet. The yield of P is 0.744, at a gas-phase conversion of 80%. The selectivity ratio is approximately 7.

A height to diameter ratio of 4 is chosen for the riser reactor. The catalyst particle size is assumed to be 100 μm, while a solids holdup of 0.05 is chosen, typical values for the regime under consideration. The evaluation results are given in Table 14. The yield of P is estimated to be 0.74, slightly lower than for the bubbling bed. The gas-phase conversion is 78%, while the selectivity ratio is somewhat better at 8.46. Since the riser regime does not offer any advantages in terms of an increased yield, the three-phase bubbling bed reactor is selected as the reactor of choice. The last step in the screening step can involve preliminary optimization of the phase distribution and transport attributes in the reactor. This is described below.

Table 14. Results for a Three-Phase Riser Reactor (Example 2)

H	1.72 m	Yield of P	0.74
D_T	0.43 m	x_A	0.78
d_p	100 μm	P/X	8.46
U_G	0.275 m/s	G_A	8.79 mol/m^3
U_L	0.0068 m/s	L_B	259.5 mol/m^3
ϵ_S	0.05	L_P	1109.4 mol/m^3
ϵ_L	0.55	L_X	131.1 mol/m^3
k_S	1×10^{-4} m/s		
$k_L a$	0.15 s^{-1}		

Table 15. Optimum Particle Size in a Three-Phase Bubbling Bed Reactor (Example 2)

d_p	475 μm	Yield of P	0.784
ϵ_S	0.4	P/X	6.35
$k_L a$	0.18 m/s	x_A	0.85
k_S	0.001 m/s		
a_S	5052 m^{-1}		

The catalyst particle diameter and the solid holdup have a strong effect on the hydrodynamic, mass-, and heat-transfer characteristics, and, hence, on the reactor conversion and selectivity in a fluidized-bed reactor. The gas-liquid mass-transfer resistance decreases with an increasing particle diameter because of bubble breakage, while the intraparticle diffusion resistance increases with particle diameter. Appropriate correlations relating the solid-liquid and gas-liquid mass-transfer coefficient to the particle diameter are used with the three-phase bubbling bed model to identify the optimum catalyst size for the reaction under consideration. The objective function to be maximized is the yield of P at the reactor outlet. The optimum particle size is found to be 475 μm where the yield of P is 0.784 (Table 15). Other operating conditions such as temperature, pressure, feed rates, reactor aspect ratio, and so on, may also be optimized, although that is not illustrated here.

Example 3: scale-up of a single gas-solid catalytic reaction

Consider a single gas-phase reaction catalyzed by a solid catalyst

$$A \xrightarrow{k_v} P$$

with k_v being the first-order reaction rate constant based on catalyst volume. The production reactor will be geometrically similar to the bench-scale reactor, but m times larger, and operated at the same temperature and pressure. For the conversion to be maintained constant with a scale change, we require that (Table 10)

$$\frac{N_r^l N_m^l}{N_r^l + N_m^l} = \frac{N_r^s N_m^s}{N_r^s + N_m^s} \tag{14}$$

Since the bench-scale reactor operates at the same reaction conditions as the commercial scale reactor, N_r will scale according to the relationship given in Eq. 11. Then, let the mass-transfer number N_m scale, not by the relationships given in Eqs. 12 and 13, but by a factor α, so as to satisfy Eq. 14. Substituting these scaling relationships in Eq. 14, we get

$$\alpha = \frac{N_m^l}{N_m^s} = \frac{\sqrt{m}}{\sqrt{m} + \left(\frac{N_m}{N_r}\right)^s \left(\sqrt{m} - 1\right)} \tag{15}$$

This is the required variation in N_m to maintain a constant gas conversion, and is a function of the scale ratio m and the ratio of the mass transfer to the reaction number, that is, N_m/N_r, in the bench-scale reactor. If the bench reactor operates at different reaction conditions than the commercial reactor, N_r will scale according to some expression other than Eq. 11, leading to a corresponding relationship for α, which can be readily obtained in a similar manner.

One possible way to achieve the required variation in N_m is by suitably controlling the bubble size in the production reactor. A scale-up to achieve a hydrodynamic similarity scales the bubble diameter by a factor of m. However, let the variation in d_b, required to achieve the required variation in N_m, be given by

$$\frac{d_b^l}{d_b^s} = r_d \tag{16}$$

Then, from Eqs. 5, 9, 15, and 16, and making use of the appropriate scaling relationships, we get

$$\text{If } \beta < 0.1, \qquad r_d = m^{2/3}\left(\sqrt{m} + \left(\frac{N_m}{N_r}\right)^s \left(\sqrt{m} - 1\right)\right)^{2/3} \tag{17}$$

$$\text{If } \beta > 10, \qquad r_d = m^{2/7}\left(\sqrt{m} + \left(\frac{N_m}{N_r}\right)^s \left(\sqrt{m} - 1\right)\right)^{4/7} \tag{18}$$

Figures 6a, 6b, and 6c show the variation of r_d/m and α, with the scale ratio m for three different values of $(N_m/N_r)^s$. In Figure 6a, $(N_m/N_r)^s = 0.1$, which implies that the bench-scale reactor operates in a mass-transfer limiting regime. α, as given by Eq. 15, is plotted as a function of m, at the bottom. This is the required variation in N_m to maintain the same conversion in the production reactor. The shaded region in Figure 6 indicates an α higher than that specified by Eq. 15, and will lead to a higher conversion, while that in the unshaded region will lead to a lower conversion due to mass-transfer limitations. In the upper graph, the $r_d/m = 1$ line indicates scale-up to achieve hydrodynamic similarity. For $\beta < 0.1$, r_d/m lies close to the line for hydrodynamic scale-up. This implies that if the bubble-dense phase mass transfer in the large-scale reactor is dominated by convection, a scale-up to achieve hydrodynamic similarity will also be sufficient to achieve similarity in reactor performance. On the other hand, for $\beta > 10$, r_d/m decreases sharply as the scale ratio increases. Thus, for processes where the bubble-dense phase mass transfer in the large-scale reactor is dominated by diffusion, the bubble size in the large reactor needs to be controlled carefully, and has to be less than that achieved by hydrodynamic similarity. Various means may be employed to limit the bubble size to the required value. These include using distributor plates with finer orifices (at the cost of an increased pressure drop), or using horizontal baffles or other internals such as heat transfer tubes across the reactor cross-section.

Note that controlling the bubble diameter in this way does not violate the original scale-up criteria of Eq. 1. Hydrodynamic similarity is violated only to the extent that the bubble and solids holdup in the reactor may not remain constant when scaling up, and the bubble diameter scales up, not by the scale ratio m, but by the new value r_d.

Figure 6b indicates that for a higher $(N_m/N_r)^s$, where mass transfer is not limiting as compared to the reaction, the α required for maintaining conversion is lower. For convection-limited mass transfer, the required (r_d/m) is greater

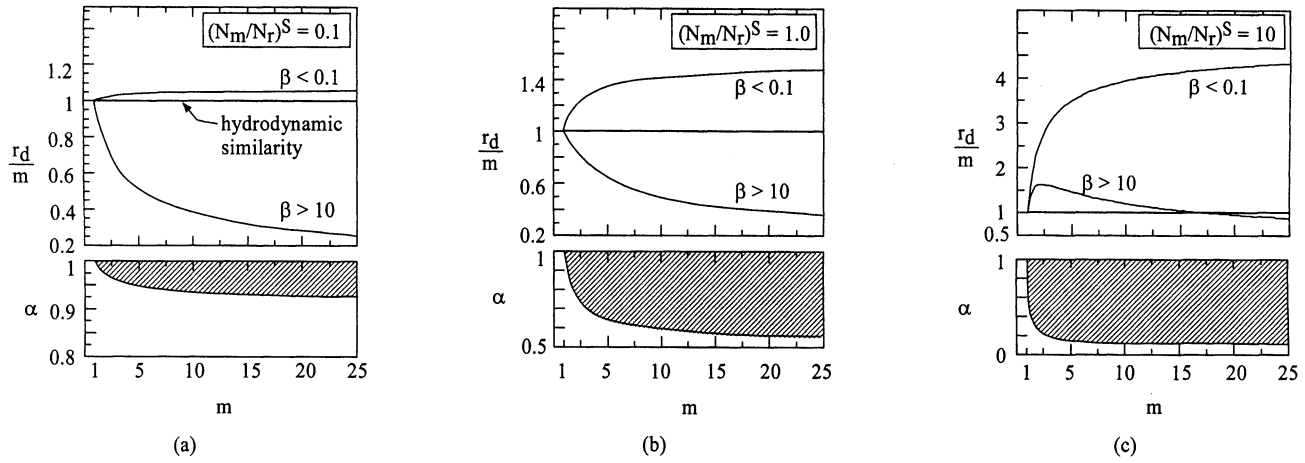

Figure 6. Required scale ratios for N_m and d_b to maintain a constant conversion during scale-up of a single catalytic reaction (Example 3).

than that achieved by hydrodynamic similarity, and bubbles may be allowed to grow to a size bigger than that achieved by hydrodynamic similarity. For diffusion limited mass transfer in the commercial reactor, however, the bubble size has to be limited to that prescribed by the lower (r_d/m) line.

For $(N_m/N_r)^s = 10$, the overall reactor performance is limited by the reaction. As indicated by the α curve in Figure 6c, the required N_m^l is only about 20% of N_m^s. The required (r_d/m) curves lie above the one for hydrodynamic similarity, irrespective of whether convection or diffusion dominates the bubble-dense phase mass transfer, except for very high scale ratios. This implies that scale-up to achieve hydrodynamic similarity will maintain (and even exceed) the conversion obtained in the bench-scale reactor. Note that for multiple reactions, this does not imply that the product distribution in the commercial reactor will be maintained as in the bench-scale reactor.

Now consider a numerical example which illustrates the above scale-up methodology. Consider the reaction shown earlier, with a first-order rate constant of $k_v = 2\ s^{-1}$. The bench-scale reactor is 15 cm in diameter, and operates at a gas superficial velocity of $U_G = 0.104$ m/s, giving a gas-phase conversion of 76%. The various reactor attributes and expanded bed characteristics are given in column 2 of Table 16. Column 3 shows the reactor characteristics and the conversion for a large-scale reactor, which is hydrodynamically similar to the bench-scale reactor, with the scale-up done according to the relationships given in Eqs. 1 to 4. The particle diameter is adjusted so as to scale up the minimum fluidization velocity U_{mf} by $\sqrt{m}$, as prescribed in Eq. 3. The expanded bed height H is determined by the hydrodynamic relationships given in Table 2. The conversion in the commercial-scale reactor ($x_A = 35\%$) clearly falls well short of that obtained at the bench scale. Figure 7 plots the reactor conversion as a function of the dimensionless reactor height Z for the bench-scale reactor ($m = 1$) and for the commercial-scale reactor with the bubble diameter being scaled to achieve hydrodynamic similarity ($m = 20$; $r_d = 20$), the second curve being significantly below the first. To achieve similarity in the reactor conversion, we proceed as follows. Since $m = 20$, and $(N_m/N_r)^s = 0.77$, the required value of α, as given by Eq. 15 is 0.6. Thus, an $N_m^l = 1.62$ will achieve a similarity in conversion. This can be obtained at an r_d of 9.8. Thus, the bubble diameter in the commercial-scale reactor ($D_T = 13$ m) has to be limited to a value of about 0.43 m. The reactor conversion as a function of the bed height in Figure 7 then reproduces the curve for the bench-scale reactor.

Example 4: scale-up of a parallel gas-solid catalytic reaction

Consider a parallel catalytic reaction scheme as shown

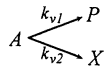

Table 16. Scale-Up of a Gas-Solid Catalytic Reaction (Example 3)

		m = 20 (Commercial Scale)	
	$m = 1$ (Small Scale)	Hydrodynamic Similarity	Matching Conversion
Reactor Geometry and Phase Flows			
D_T (m)	0.15	3.13	3.13
H (m)	0.38	7.62	8.39
wt (kg)	4	32000	32000
U_{mf} (m/s)	0.0031	0.0137	0.0137
U_G (m/s)	0.104	0.462	0.462
u_b (m/s)	0.56	2.53	2.50
Phase Distribution			
d_p (μm)	60	125	125
d_b (m)	0.044	0.88	0.43
ϵ_b	0.17	0.17	0.25
ϵ_S	0.45	0.45	0.41
Transport Attributes			
k_{be} (m/s)	0.029	0.023	0.025
a (m^{-1})	24.1	1.21	3.52
Dimensionless No. and Reactor Performance			
N_r	**3.33**	**14.9**	**14.9**
N_m	**2.57**	**0.455**	**1.62**
x_A	**0.76**	**0.35**	**0.76**

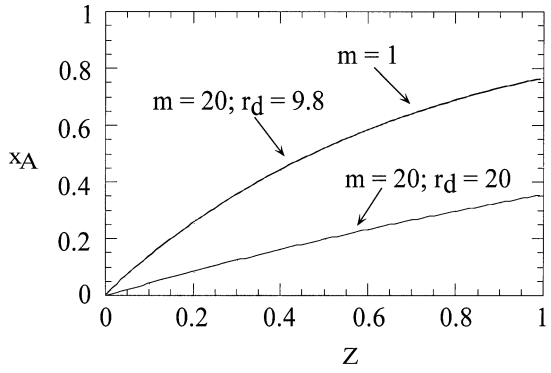

Figure 7. Reactor performance for Example 3 for scale-up according to various criteria.

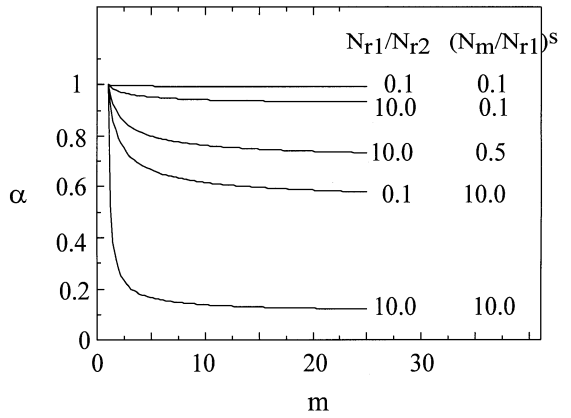

Figure 8. Required scale ratios for *Nm* to maintain a constant product yield during scale-up of a parallel catalytic reaction scheme (Example 4).

where k_{v1} and k_{v2} are the first-order rate constants based on catalyst volume. The desired product is P, whereas X is the undesired byproduct. For the simplified two-phase model, the analytical expressions for the conversion of A, the yield of P (defined as the amount of P produced divided by the amount of A fed), and the selectivity to P (defined as the amount of P produced divided by the amount of A reacted) are given in Table 10. Here, N_{r1} and N_{r2} are the dimensionless reaction numbers for the desired and the undesired reaction, respectively. The performance index to be maintained constant during scale-up is chosen to be the product yield y_P.

If the bench-scale reactor operates at the same reaction conditions as the commercial-scale reactor, N_{r1} and N_{r2} will scale according to the relationship given in Eq. 11. The required variation in N_m in order to maintain a constant y_P for a scale ratio of m is then given by

$$\alpha = \frac{N_m^l}{N_m^s} = \frac{\sqrt{m}\,(1+1/r_{12})}{\sqrt{m}\,(1+1/r_{12}) + \left(\frac{N_m}{N_{r1}}\right)^s \left(\sqrt{m}-1\right)} \qquad (19)$$

Here, r_{12} is the ratio of the reaction numbers for the desired and undesired reactions, that is N_{r1}/N_{r2}, or simply k_{v1}/k_{v2}. Then, r_d, the required ratio in which the bubble diameter should scale in order to achieve the N_m^l given by the above equation, is given by

$$\text{If } \beta < 0.1, \quad r_d = m^{2/3}\left(\frac{\sqrt{m}\,(1+1/r_{12}) + \left(\frac{N_m}{N_{r1}}\right)^s \left(\sqrt{m}-1\right)}{(1+1/r_{12})}\right)^{2/3} \qquad (20)$$

$$\text{If } \beta > 10, \quad r_d = \left(\frac{m(1+1/r_{12}) + \sqrt{m}\left(\frac{N_m}{N_{r1}}\right)^s \left(\sqrt{m}-1\right)}{(1+1/r_{12})}\right)^{4/7} \qquad (21)$$

Figure 8 plots α as a function of the scale ratio m with r_{12}, and $(N_m/N_{r1})^s$ as parameters. For a given r_{12}, α decreases as $(N_m/N_{r1})^s$ increases, that is, as mass-transfer limitations in the bench-scale reactor decrease. Similarly, for a given $(N_m/N_{r1})^s$, α decreases as r_{12} increases, that is, as the desired reaction becomes faster relative to the undesired one.

Let us now consider a numerical example to illustrate the scale-up for this reaction scheme. Consider a bench-scale reactor operating at $N_{r1} = 10$, $N_{r2} = 1$, and $N_m = 5$. The conversion of A, as calculated from the expressions given in Table 10, is 96%, whereas the yield of P, y_P, is 88% (Table 17). The reactor is to be scaled up by a factor of 16. The new reaction numbers are then $N_{r1} = 40$ and $N_{r2} = 4$. Since no other information about the bench-scale reactor is assumed, the value of β, that is, the relative extent of the diffusion vs. the convection component in the bubble-dense phase mass-transfer coefficient is unknown. Hence, we examine hydrodynamic similarity under the two extreme cases of $\beta < 0.1$ and $\beta > 10$. For these two cases, N_m scales, as given by Eqs. 12 and 13, respectively. The reactor performance under hydrodynamic similarity is tabulated in columns 3 and 4 of Table 17. It is seen that if convection dominates the mass-transfer coefficient in the commercial-scale reactor, the conversion of A, as well as the yield of P, increases over that observed in the bench-scale reactor. If, however, the mass transfer in the commercial-scale reactor is dominated by diffusion, the conversion and yield fall well short of those observed on the bench scale. To maintain reactor yield, the required value of

Table 17. Scale-Up of a Parallel Gas-Solid Catalytic Reaction (Example 4)

		$m = 16$ (Commercial Scale)		
		Hydrodynamic Similarity		Reaction Similarity
	$m = 1$ (Bench Scale)	If $\beta < 0.1$ $\alpha = 1$	If $\beta > 10$ $\alpha = 0.125$	$\alpha = 0.745$
N_{r1}	10	40	40	40
N_{r2}	1	4	40	4
N_m	5	5	0.625	3.725
x_A	0.96	0.98	0.46	0.96
y_P	0.88	0.89	0.41	0.88

α can be obtained from Figure 8. For $r_{12} = 10$, $(N_m/N_{rl})^s = 0.5$, and $m = 16$, we have $\alpha = 0.74$. This gives $N_m^l = 72$. A commercial-scale reactor operating under these conditions maintains the yield of P at 88%.

The previous two examples illustrated how a modification of the scale-up rules for hydrodynamic similarity can achieve a similarity in the reactor performance as well. The next example, which illustrates the screening as well as the scale-up steps, uses a somewhat different scale-up strategy than what was used for the previous two examples.

Example 5: oxidation of o-xylene to phthalic anhydride

Consider the highly exothermic catalytic oxidation of o-xylene to phthalic anhydride. A simplified reaction scheme for this reaction is given below (Froment, 1967)

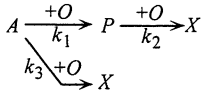

Here, A represents o-xylene, O is oxygen, P is phthalic anhydride, and X is the final oxidation products CO and CO_2 lumped together. O-xylene is vaporized and mixed with air before entering the reactor. Its concentration is kept below 1 mol. % in order to stay under the explosion limit. Because of the large excess of oxygen, the rate expressions for all three reactions can be considered to be of first order with respect to the corresponding reactant. The rate constants as functions of temperature, as well as the heats of reaction, are given in Table 18a. The operating pressure is nearly atmospheric. The feed temperature is 620 K. The contact times are of the order of 1 s. As is clear from the reaction scheme, the yield of P increases with the extent of reaction up to a point, after which X is the major product. The objective is to synthesize a gas-solid catalytic reactor to produce 500 tonnes/y of P, while maintaining a high selectivity to P.

Screening

Step 1: The ratio [amount of P formed]/[amount of X formed] is chosen as the performance index.

Step 2: Generic model. A network of tanks in series is chosen to model the reactions.

Step 3: Sensitivity model. The parameters of interest are the gas-solid mass-transfer coefficient $k_S a_S$, the particle diameter d_p, the reactor temperature T, and the number of tanks N in the model.

Step 4: Generate Base Case. A packed-bed reactor without any heat removal mechanism (Figure 1i) is chosen as the base case for this reaction. The base case parameters are summarized in Table 18a. A gas-phase residence time of 1 s leads to essentially complete conversion, and a very low selectivity to P. This is because of the enormous temperature rise along the reactor length, which favors the undesirable reactions more than the desired reaction. The maximum selectivity ratio of 0.88 in a packed-bed reactor is obtained with a residence time of 0.5 s.

Step 5: Screen Parameters. The results of the screening procedure are shown in Table 18b. The performance index P/X, and the reactor volume V, required to produce 500 tonnes/y of P, are shown in columns 2 and 3, respectively. The parameters $k_S a_S$, d_p, and the highest temperature in the reactor T_{high}, along with their sensitivity to the performance index, are shown in the remaining columns. No diffusion limitations are encountered inside the catalyst. The last column identifies the corresponding reactor type for each iteration.

Table 18. (a) Base-Case Parameters for Example 5: Oxidation of o-Xylene to Phthalic Anhydride; (b) Sensitivity Analysis for Example 5

(a)

F_G	1 m³/s	k_1	$4.2\times10^6\ e^{-112{,}000/RT}$ (m³/kg·s)
τ_G	1 s	k_2	$2.0\times10^7\ e^{-140{,}000/RT}$ (m³/kg·s)
ϵ_G	0.4	k_3	$2\times10^6\ e^{-130{,}000/RT}$ (m³/kg·s)
ϵ_S	0.6	*Feed Conditions*	
k_S	1×10^{-3} m/s	G_A	0.2 mol/m³
ΔH_1	-1.28×10^6 J/mol	G_B, G_P, G_X	0 mol/m³
ΔH_2	-4.5×10^6 J/mol	T_{feed}	620 K
ΔH_3	-1×10^6 J/mol	$T_{coolant}$	620 K

(b)

	P/X	V (m³)	$k_S a_S$ (s⁻¹)	$\bar{\Psi}$ ($k_S a_S$)	d_p (μm)	$\bar{\Psi}$ (d_p)	T_{high} (K)	$\bar{\Psi}$ (T)	N	Corresponding reactor type
1		2.0	0.72		5,000		678		8	Packed reactor without heat transfer
	0.88			−1.14		−1.23		**−14**		
2		2.5	0.72		5,000		621.3		8	Multitubular packed bed immersed in salt bath
	8.40		↓	**0.23**	↓	**−0.35**		−0.05	↓	
3		1.33	12		200		631.3		1	Bubbling fluidized bed with internal heat transfer
	11.86		↓	0.02	↓	−0.022		**−9**	↓	
4		1.7	18		100		622.3		8	Riser reactor
	21			0.01		−0.01		**−0.03**		

For the adiabatic packed bed, even with a shorter contact time, the temperature rise across the bed is unacceptable ($T_{high} = 678$ K). $\overline{\Psi}(T)$ is the dominant sensitivity, indicating that heat removal should be the priority. Iteration 2 therefore considers a multitubular packed-bed reactor. 2,500 tubes, each 1.4 m long and 3 cm in diameter, are arranged in a shell-and-tube heat exchanger type construction. Circulating molten salt at 620 K can be used outside the tubes to manage the heat of reaction. A selectivity of 8.4 is obtained with a gas-phase residence time of 1 s. The operation is essentially isothermal ($T_{high} = 621.3$ K). $\overline{\Psi}(d_p)$ is the dominant sensitivity, indicating that using a smaller diameter catalyst will improve the selectivity. However, pressure drop considerations do not allow the catalyst particle diameter to be reduced much further. Here, we note that a fluidized mode of operation can handle much smaller particle sizes, and also has better heat- and mass-transfer characteristics. Iteration 3 therefore considers the use of a bubbling fluidized reactor to carry out the above reaction. The catalyst diameter is reduced to 200 μm, and the phase distribution and transport parameters are changed to typical values observed in fluidized beds. N, the number of tanks in the reactor model, is changed to 1 to reflect the extensive backmixing observed in bubbling fluidized beds. At the lower particle diameter, iteration 3 shows an improved selectivity ($P/X = 11.86$). The reactor volume and the gas feed rate required are also lower than for the earlier iterations. However, due to the limited heat-transfer area available, there is still a significant temperature rise ($T_{high} = 631.3$ K). If this is acceptable, the bubbling fluidized bed is an attractive reactor choice. However, the dominant temperature sensitivity ($\overline{\Psi}(T) = -9$) indicates that the selectivity can be further improved by operating at a lower temperature. Iteration 4 therefore considers operating the fluidized-bed reactor as a riser reactor. Here, a much higher heat removal rate can be achieved by continuously removing the hot catalyst particles from the reactor. The catalyst diameter is decreased to 100 μm to facilitate particle carryover. The temperature rise along the reactor length is therefore lower ($T_{high} = 622.3$ K). A high selectivity ratio of 21 is obtained for such an operation. The short gas-phase residence time of 1 s also makes this operation attractive.

Step 6: Identify Reactor Type. The above set of parameters indicate a riser reactor (Figure 1vi) with a 30% solid holdups and a high gas-solid mass-transfer coefficient. There is a continuous carryover of solids out of the reactor. The required reactor volume and gas feed rate are intermediate to those for the packed beds and the bubbling fluidized bed. If a 10 degree temperature rise across the reactor is acceptable, a bubbling fluidized bed (Figure 1iii) may be used to carry out the reaction (Iteration 3).

The two candidate reactors recommended by the screening procedure are a bubbling fluidized bed, and a dense-phase riser reactor. These are evaluated more carefully using specific models, described previously, for each candidate reactor or operating flow regime. The two-phase bubbling bed model is used to simulate the former, whereas a two-phase plug-flow model is used to represent the riser reactor. For the bubbling fluidized bed, the voidage and the height to diameter ratio at minimum fluidization was chosen to be 0.55 and 5, respectively. From the hydrodynamic relations for the two-phase model given in Table 2, it is clear that a smaller catalyst diameter leads to a lower U_{mf} and, hence, a lower gas-emulsion mass-transfer coefficient k_{be}, and requires a higher catalyst loading (or a larger reactor) for the required production of P. Note that the reactions are slow enough that a change in catalyst size does not significantly affect the catalyst effectiveness. Thus, for a catalyst diameter of 200 μm and a corresponding k_{be} of 0.019 m/s, the bubbling bed requires a catalyst loading of 1,500 kg with an expanded bed volume of 48 m^3 for producing 500 tonnes/y of P. The selectivity ratio is also low at 7.9. With a higher catalytic diameter of 400 μm, the gas-emulsion mass-transfer coefficient is higher ($k_{be} =$ 0.019 m/s). The results for this simulation are shown in Table 19. A catalyst loading of 800 kg in a bed volume of 2.14 m^3 (a catalyst density of 372 kg catalyst/m^3 reactor) can produce the required throughput with a selectivity ratio of 12.25. Comparing the phase holdups and the gas velocity to the typical values given in Table 7, it is seen that the bed operates in the turbulent regime. With an internal heat-transfer area of 10 m^2 and a bed to surface heat-transfer coefficient of 800 W/m^2 K, the bed temperature is seen to be 637.4 K. Thus, internal heat transfer is inadequate for achieving isothermal operation. An alternate way to manage the heat of reaction is to use a circulating solids system, such as a dense-phase riser reactor.

Table 19. Results for a Turbulent Fluidized-Bed Reactor (Example 5)

H	2.3 m	d_b	0.46 m
D_T	1.08 m	k_{be}	0.051 m/s
U_G	1.29 m/s	a	12.83 m^{-1}
d_p	400 μm	P/X	12.25
ϵ_S	0.31	x_A	0.51
ϵ_b	0.43	G_A	0.1 mol/m^3
ϵ_e	0.56	G_P	0.0924 mol/m^3
wt	372 kg/m^3	G_X	0.0076 mol/m^3
		T_{out}	637.4 K

Table 19 shows the simulation results for such a reactor, with a height to diameter ratio of 10. The absence of a bubble phase implies that we do not have to worry about deteriorating bubble-emulsion contact with decreasing particle size. In fact, the gas-solid mass-transfer coefficient k_S is expected to increase with decreasing particle size, although such a correlation was not explicitly incorporated into the model. A value of 0.001 m/s was chosen for k_S, which is typical for the reactor conditions under consideration. The high heat capacity of the circulating solids allows excellent heat transfer, leading to almost isothermal operation ($T_{high} = 622$ K). A better gas solid contact and temperature control, and lower backmixing than in the turbulent bed reactor leads to a higher

Table 20. Results for a Dense-Phase Riser Reactor (Example 5)

H	6.73 m	k_S	0.001 m/s
D_T	0.67 m	a_S	12,000 m^{-1}
U_G	3.37 m/s	P/X	24.6
U_S	0.14 m/s	x_A	0.55
d_p	100 μm	G_A	0.0906 mol/m^3
ϵ_S	0.2	G_P	0.0974 mol/m^3
ϵ_G	0.8	G_X	0.0039 mol/m^3
wt	240 kg/m^3	T_{out}	623.2 K

selectivity ($P/X = 24.6$), using a lower catalyst density in the bed (240 kg catalyst/m^3 reactor), at about the same level of conversion of A. A dense-phase riser reactor is thus most suitable for the reaction under consideration. The operating conditions and the phase distribution in the reactor can be optimized by incorporating correlations between the phase distribution and transport parameters.

Scale-up. Once the reactor type and the desired flow regime has been chosen, the commercial reactor may be designed by scaling up from a bench-scale or pilot-plant reactor. Let us focus on the bubbling fluidized bed with internal heat transfer. The reactor is assumed to operate at the temperature of 637.4 K, close to that found in the screening step. The bench-scale reactor is 11.6 cm in diameter, and operates with a total catalyst loading of 0.8 kg, a gas superficial velocity of 0.093 m/s, and an o-xylene concentration of 0.2 mol/m^3 in the feed gas, to give a gas-phase conversion of 71%, and a 92% selectivity to the desired product P. This is to be scaled up to a commercial reactor producing 500 tonnes/yr of P, while maintaining the selectivity at 92%. If the conversion and selectivity are maintained at the values obtained in the bench scale, the required production rate can be achieved by scaling the reactor by a factor of 16.

The analytical expressions for the conversion of A and the yield and selectivity of P, based on the simplified, two-phase model described earlier, are given in Table 10. The scale-up criteria to maintain a constant conversion of A can be obtained as in Example 3, and is given by Eq. 15.

Let us examine the scale-up criteria for achieving a similarity in the selectivity to P, s_P. If the bench-scale reactor operates at the same reaction conditions as the commercial-scale reactor, N_{r1} and N_{r2} will scale by $\sqrt{m}$. If N_m scales by the ratio α in order to maintain a constant y_P, the value of α can be obtained by solving the following equation

$$\frac{\exp\left(\dfrac{N_m^2(N_{r1}-N_{r2}+N_{r3})}{(N_m+N_{r2})(N_m+N_{r1}+N_{r3})}\right)-1}{\exp\left(-\dfrac{N_m(N_{r1}+N_{r3})}{N_m+N_{r1}+N_{r3}}\right)-1} = \frac{\exp\left(\dfrac{\alpha^2 N_m^2\sqrt{m}\,(N_{r1}-N_{r2}+N_{r3})}{\left(\alpha N_m+\sqrt{m}\,N_{r2}\right)\left(\alpha N_m+\sqrt{m}\,N_{r1}+\sqrt{m}\,N_{r3}\right)}\right)-1}{\exp\left(-\dfrac{\alpha N_m\sqrt{m}\,(N_{r1}+N_{r3})}{\alpha N_m+\sqrt{m}\,N_{r1}+\sqrt{m}\,N_{r3}}\right)-1} \tag{22}$$

However, it can be shown that the above equation has no solution for α, for values of m, N_m^s, N_{r1}^s, N_{r2}^s, and N_{r3}^s of this example. This implies that the yield cannot be maintained constant as the reactor scale changes, if N_{r1}^s, N_{r2}^s and N_{r3}^s scale by $\sqrt{m}$.

One way to achieve a similarity in product yield is to operate the commercial-scale reactor at the same values of N_{r1}, N_{r2}, N_{r3}, and N_m, as in the bench-scale reactor. Since all the dimensionless numbers in the reactor model are held constant, the product distribution in the commercial reactor is expected to be equal to that obtained in the bench-scale reactor. The three reaction numbers may be held constant with a scale change by changing the reaction conditions so as to suitably change the reaction rate constants, k_{v1}, k_{v2}, and k_{v3}. However, this may be difficult because the rate constants have a different dependence on temperature. Another way is to operate at a lower total catalyst loading than that recommended by the scale-up criteria of Eq. 4, while still scaling the reactor diameter by m. This reduces the expanded bed height, and allows the N_r^s to be held constant. Let us consider scaling up the phthalic anhydride reactor in this manner.

A few important reactor attributes and bed characteristics of the bench scale, as well as the commercial reactor are given in column 2 of Table 21. The bench-scale reactor is to be scaled up by a factor of 16. Columns 3, 4, and 5 of Table 21 show the reactor performances for reactors scaled up according to three different criteria. Column 3 shows the reactor characteristics for a commercial-scale reactor, which is hydrodynamically similar to the bench-scale reactor, with the scale-up done according to the relationships given in Eqs. 1 to 4. The conversion in the commercial-scale reactor ($x_A = 56\%$), as well as the selectivity to the product ($s_P = 72\%$) fall well short of those obtained at the bench scale. Figure 9 plots the conversion of A and the selectivity to P, as a function of the dimensionless reactor height Z. The solid lines indicate the gas conversion, whereas the dashed lines indicate s_P obtained at different scales and for different scale-up criteria, as indicated in the figure. The curves for $m = 1$ indicate the bench-scale reactor. Column 4 of Table 21 indicates a commercial-scale reactor scaled up so as to maintain a constant conversion of A. This is obtained at an α of 0.48, as given by Eq. 15. The required bubble ratio is $r_d = 12.2$. The conversion curve in Figure 10 for this case overlaps the conversion curve for the bench-scale reactor. The selectivity curve however still lies well below the selectivity curve for the bench scale reactor.

The conversion, as well as the selectivity, can be matched by operating the commercial-scale reactor at the same values of N_{r1}, N_{r2}, N_{r3}, and N_m, as the bench-scale reactor. To achieve this, the reactor diameter is scaled by the same factor used to achieve a similarity in conversion, but the total catalyst loading is scaled by $m^{5/2}$, rather than by m^3. This maintains constant reaction numbers through the scale change. To maintain a constant mass-transfer number as well, the bubble diameter is scaled by a ratio $r_d = 8$. The bed characteristics and the reactor performance for this case is shown in column 5 of Table 21. As can be seen, the conversion and product selectivity are the same as those obtained at the bench scale. The curves for x_A and s_P in Figure 9 for such a scale-up reproduce the curves for the bench-scale reactor, as expected. Although scaling the bubble diameter by a ratio smaller than the reactor scale ratio m may be impractical, this approach illustrates the potential for maintaining reactor performance, as well as the product distribution as the reactor scale changes. The selectivity is expected to drop somewhat, in case the bubble diameters cannot be maintained at a ratio of $r_d = 8$.

Conclusions

After discovering a new reaction route or a novel catalyst for a desirable chemical, the next task facing a reaction engi-

Table 21. Scale-Up of o-Xylene to Phthalic Anhydride Reaction (Example 5)

		$m = 16$ (Commercial Scale)		
	$m = 1$ (Small Scale)	Hydrodynamic Similarity	Matching Conversion	Matching Selectivity and Conversion
		Reactor Geometry and Catalyst Loading		
D_T (m)	0.116	1.85	1.85	1.85
H (m)	0.145	2.33	2.42	0.80
U_G (m/s)	0.093	0.372	0.372	0.372
wt (kg)	0.8	3276.8	3276.8	819.2
		Phase Distribution		
d_p (μm)	100	200	200	200
d_b (m)	0.021	0.336	0.257	0.08
		Dimensionless Numbers and Reactor Performance		
N_{r1}	2	8	8	2
N_{r2}	0.05	0.2	0.2	0.05
N_{r3}	0.075	0.3	0.3	0.075
N_m	3	0.907	1.45	3
r_d	—	16	12.2	3.8
$\boldsymbol{x_A}$	**0.71**	**0.56**	**0.71**	**0.71**
$\boldsymbol{s_P}$	**0.92**	**0.72**	**0.76**	**0.92**

neer is to select the best reactor type and scale it up for commercial production. Normally, little is known about the intrinsic kinetics, and there is much uncertainty about the chemical and physical properties of the reaction system at the early stage of reactor development. Once a reactor type is selected, and time, effort and money has been spent on its development, there is a great deal of disincentive to investigate another reactor type. It is not surprising that reactor selection is often delegated to the most experienced engineer in the company. Yet, experience is no guarantee for success. The problem is further compounded by the unrelenting pressure to shorten the time-to-market. For these reasons, we have been working on systematic methods to aid in reaction system synthesis, focusing on extractive reaction (Samant and Ng, 1998a,b,c), reactive crystallization (Kelkar and Ng, 1999), pre-polymerization (Samant and Ng, 1999a), reactions dominated by micromixing (Samant and Ng, 1999b), and others.

This article presents such methods for fluidized catalytic reactors, with the aim of facilitating the selection and scale-up of this reactor type. In a step-by-step manner, the engineer is guided by sensitivity analysis to identify the limiting step, transport or otherwise, in the reaction system. And the reactor type, as well as reactor attributes and operating conditions, is selected to relax the limiting step(s) so as to realize the full potential of the reaction.

Instead of sensitivity tests, the dominant mechanisms can also be captured by identifying the dimensionless numbers in the governing equations for hydrodynamics and reactions. It is expected that similar reactor performance can be obtained in scaling up the bench-scale reactor to the production reactor by keeping these dimensionless numbers constant. Clearly, the transport and reaction processes in a particular system can be so complex that the governing equations may not offer a sufficiently accurate description. In such cases, the recommended scale-up criteria should only be used to provide directions for further development.

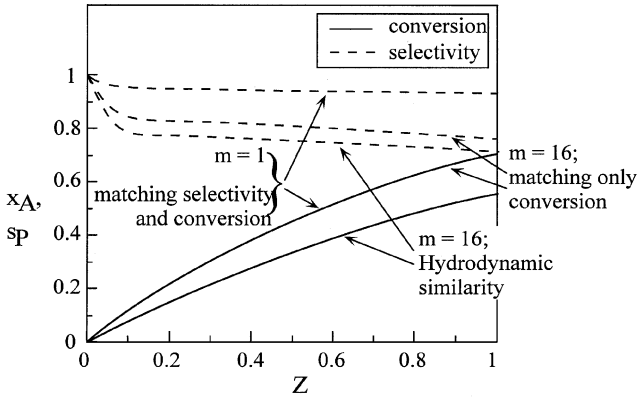

Figure 9. Reactor performance for Example 5 for scale-up according to various criteria.

Acknowledgment

The financial support of the National Science Foundation (grant no. 9807101) for this research is gratefully acknowledged.

Notation

a = interfacial area of the bubble phase, m^2/m^3
a_h = surface area for heat transfer per unit volume of reactor, m^2/m^3
a_S = solid surface area per unit volume of reactor, m^2/m^3
$A, B...$ = reactant species
Ar = Archimedes number
A_T = cross-sectional area of the bed, m^2
C_A, E_A = concentrations of species A, in the cloud phase and the dense phase, respectively, mol/m^3
d_p = diameter of (spherical) catalyst particles, m
d_b = mean bubble diameter in the bed, m
D = effective diffusion coefficient, m^2/s
D_T = bed diameter, m
f_b = fraction of gas flow carried by the bubble phase
F_G, F_L = flow rate of gas and liquid phase through the reactor, m^3/s

G_A, L_A, S_A = concentrations of species A, in the gas (bubble) phase, the liquid phase, and at the catalyst surface, rrespectively, mol/m^3

$\overline{G}_A$, $\overline{E}_A$ = dimensionless bubble phase and dense phase concentrations, respectively, mol/m^3

G_S = solids flow rate, kg/m^{2}s

H = expanded bed height, m

H_i = solubility coefficient for species i, (mol/m^3)$_{\text{gas}}$/mol/m^3)$_{\text{liquid}}$

ΔH_k = heat of reaction for the kth reaction, J/mol·K

$k_{be}a$,$k_{be}a$,$k_{ce}a$ = bubble-dense phase, bubble-cloud phase, and cloud-dense phase mass-transfer coefficient, respectively, s^{-1}

k_L = overall gas-liquid mass-transfer coefficient, m/s

k_S = solid-liquid mass-transfer coefficient, m/s

k_v = reaction rate constant based on catalyst volume, s^{-1}

L = characteristic length scale of the reactor, m

m = scale ratio

n = Richardson Zaki index

N = total number of perfectly mixed tanks in series in the generic reactor model

N_r = dimensionless reaction number

P,Q = products of reaction

r_d = required scale-up ratio for bubble diameter

s_P = selectivity to desired product

u_b = bubble rise velocity, m/s

U = overall heat-transfer coefficient, W/m^2·K

U_G = superficial gas velocity, m/s

U_{mf} = minimum fluidization velocity, m/s

U_t = particle terminal settling velocity, m/s

w = catalyst loading per unit volume of reactor, kg/m^3

wt = total catalyst loading in the reactor, kg

x_A,x_B = conversion of reactant A and B, respectively

X = undesirable product of reaction

y_P = yield of desired product

z, Z = dimensional and dimensionless distance along reactor height

α = required scale-up ratio for the mass-transfer number N_m

β = ratio of diffusion component to the convection component in the mass-transfer coefficient

ϵ_S, ϵ_L, ϵ_G = solid, liquid and gas-phase holdup in the reactor

ϵ_b, ϵ_e, ϵ_c, ϵ_w = volume fraction of the bubble, emulsion, cloud, and wake phases in the fluidized-bed reactor

ϵ_{bs}, ϵ_{es}, ϵ_{cs}, ϵ_{ws}, = volume fraction of the bubble, emulsion, cloud, and wake phases occupied by solids

ϵ_{mf} = bed voidage at minimum fluidization

ϕ = particle sphericity

Φ_A, Φ_{Ab}, Φ_{Ac}, Φ_{Ae} = rate of consumption of species A in the reactor, the bubble phase, the cloud phase, and the dense phase, respectively, mol/m^3·s

η = catalyst effectiveness factor

μ = viscosity, Pa·s

ρ = density, kg/m^3

$\overline{\Psi}(\alpha_i)$ = normalized sensitivity of the performance index to the parameter α_i

Subscripts and superscripts

0 = pertaining to inlet (feed) conditions

b = bubble phase

c = cloud phase

e = emulsion phase

f = feed condition

G = gas phase

L = liquid phase

mf = minimum fluidization

S = solid phase

w = wake phase

Literature Cited

Bergougnou, M. A., C. L. Briens, and D. Kunii, "Design Aspects of Industrial Fluidized Bed Reactors. Research Needs. Selected Subjects," *Chemical Reactor Design and Technology*, H. I. De Lasa, ed., Martinus Nijhoff Publishers, Dordrecht, The Netherlands, 305 (1986).

Bhatia, V. K., and N. Esptein, *Fluidization and Its Applications*, H. Angelino, J. P. Couderc, H. Gilbert, and C. Laguerie, eds., Cepadues-Editions, Toulouse, France, 380 (1974).

Carson, J. W., and J. Marinelli, "Characterize Bulk Solids to ensure Smooth Flow," *Chem. Eng.*, **101**(4), 78 (1994).

Chen, L. H., and J. R. Too, "Fluidized Bed Models," *Encyclopedia of Fluid Mechanics Vol. 4: Solids and Gas-Solid Flow*, N. P. Cheremisinoff, ed., Gulf Publishing Co., Houston, p. 1161 (1986).

Davidson, J. F., and D. Harrison, *Fluidized Particles*, Cambridge Univ. Press, London, p. 50 (1963).

Davidson, J. F., and D. Harrison, *Fluidization*, Academic Press, London (1971).

Fan, L. S., *Gas-Liquid-Solid Fluidization Engineering*, Butterworths, Boston (1989).

Fane, A. G., and C. Y. Wen, "Fluidization Bed Reactors," *Handbook of Multiphase Systems*, G. Hetsroni, ed., Hemisphere Publishing Corp., Washington, p. 8–104 (1982).

Froment, G. F., "Fixed-bed Catalytic Reactors. Current Design Status," *Ind. Eng. Chem.,* **59**, 18 (1967).

Glicksman, L. R., "Scaling Relationships for Fluidized Beds," *Chem. Eng. Sci.*, **39**, 1373 (1984).

Glicksman, L. R., M. Hyre, and K. Woloshun, "Simplified Scaling Relationships for Fluidized Beds," *Powder Technol.*, **77**, 177 (1993).

Grace, J. R., "Evaluation of Models for Fluidized Bed Reactors" *Fluidization: Fundamental Studies, Solid-Fluid Reactions, and Applications*, AIChE Symp. Ser., A. M. Al-taweel, H. Littman, eds., Vol. 67, No. 116, AIChE, New York, p. 159 (1971).

Grace, J. R., Fluidized-Bed Hydrodynamics" *Handbook of Multiphase Systems*, G. Hetsroni, ed., Hemisphere Publishing Corp., Washington, p. 8-1 (1982).

Grace, J. R., "Generalized Models for Isothermal Fluidized Bed Reactors," *Recent Advances in the Engineering Analysis of Chemically Reacting Systems*, L. K. Doraiswamy, ed., Wiley Eastern Ltd., New Delhi, p. 237 (1984).

Grace, J. R., "Fluid Beds as Chemical Reactors," *Gas Fluidization Technology*, D. Geldart, ed., Wiley, Chichester, U.K., p. 285 (1986).

Harrison, D., and J. R. Grace, "Fluidized Beds With Internal Baffles," *Fluidization*, J. F. Davidson and D. Harrison, eds., Academic Press, London, 599 (1971).

Horio, M., and C. Y. Wen, "An Assessment of Fluidized Bed Modeling," *Fluidization Theories and Applications,* AIChE Symp. Ser., J. S. Halow, ed., Vol. 73, No. 161, AIChE, New York, p. 9 (1977).

Horio, M., A. Nonaka, T. Sawa, and E. Muchi, "A New Similarity Rule for Fluidized Bed Scale-up," *AIChE J.*, **32**, 1466 (1986).

Horio, M., H. Ishii, Y. Kobukai, and N. Yamanishi, "A Scaling Law for Circulating Fluidized Beds," *J. Chem. Eng. Jpn.*, **22**, 587 (1989).

Ihara, T., A. Kayou, and Y. Natori, "Scaleup Study of the Turbulent Fluidized Bed Reactor," *AIChE Symp. Ser.*, No. 313, 81 (1996).

Jazayeri, B., "Successfully Scale Up Catalytic Gas-Fluidized Beds," *Chem. Eng. Prog.*, 26 (April 1995).

Kelkar, V. V., and K. M. Ng, "Screening Procedure for Synthesizing Isothermal Multiphase Reactors," *AIChE J.*, **44**, 1563 (1998).

Kelkar, V. V., and K. M. Ng, "Design of Reactive Crystallization Systems Incorporating Kinetics and Mass Transfer Effects," *AIChE J.*, **45**, 69 (1999).

Kelkar, V. V., and K. M. Ng, "Screening Multiphase Reactors for Nonisothermal Multiple Reactions," *AIChE J.*, **46**, 389 (2000).

Krishna, R., and S. T. Sie, "Strategies for Multiphase Reactor Selection," *Chem. Eng. Sci.*, **49**, 4029 (1994).

Kunii, D., and O. Levenspiel, *Fluidization Engineering*, 2nd ed., Wiley, New York (1991).

Kwauk, M., ed., *Fast Fluidization*, Academic Press, San Diego (1994).
Matsen, J., "Scale-up of Fluidized Bed Processes: Principles and Practice," *Powder Technol.*, **88**, 237 (1996).
Matsen, J. M., and B. L. Tarmy, "Scale-up of Laboratory Fluid-Bed Data: Significance of Slug Flow," *Chem. Eng. Prog. Symp. Ser.*, **66**, 1 (1970).
Orcutt, J. C., J. F. Davidson, and R. L. Pigford, "Reaction Time Distributions in Fluidized Catalytic Reactors," *Fluidization*, Chem. Eng. Prog. Symp. Ser., F. A. Zenz, ed., Vol. 58, No. 38, AIChE, New York, p. 1 (1962).
Papa, G., and F. A. Zenz, "Optimize Performance of Fluidized Bed Reactors," *Chem. Eng. Prog.*, 32 (Apr. 1995).
Samant, K. D., and K. M. Ng, "Synthesis of Extractive Reaction Processes," *AIChE J.*, **44**, 1363 (1998a).
Samant, K. D., and K. M. Ng, "Effect of Kinetics and Mass Transfer on Design of Extractive Reaction Systems," *AIChE J.*, **44**, 2212 (1998b).
Samant, K. D., and K. M. Ng, "Design of Multistage Extractive Reaction Processes," *AIChE J.*, **44**, 2689 (1998c).
Samant, K. D., and K. M. Ng, "Synthesis of Prepolymerization Stage in Polycondensation Processes," *AIChE J.*, **45**, 1808 (1999a).
Samant, K. D., and K. M. Ng, "Development of Liquid Phase Agitated Reactors: Synthesis, Simulation and Scaleup," *AIChE J.*, **45**, 2353 (1999b).
Van Swaaij, W. P. M., "Chemical Reactors," *Fluidization*, J. F. Davidson, R. Clift, and D. Harrison, eds., Academic Press Inc., London, p. 595 (1985).
Varma, Y. B. G., "Pressure Drop of the Fluid and the Flow Patterns of the Phases in Multistage Fluidization," *Powder Technol.*, **12**, 167 (1975).
Weissermal, K., and H. J. Arpe, *Industrial Organic Chemistry*, VCH, New York (1993).
Wen, C. Y., "Flow Regimes and Flow Models for Fluidized Bed Reactors," *Recent Advances in the Engineering Analysis of Chemically Reacting Systems*, L. K. Doraiswamy, ed., Wiley Eastern Ltd., New Delhi, 256 (1984).
Whitehead, A. B., "Some Problems in Large-Scale Fluidized Beds," *Fluidization*, J. F. Davidson and D. Harrison, eds., Academic Press, London, 781 (1971).
Yates, Y. G., *Fundamentals of Fluidized Bed Chemical Processes*, Butterworths, London (1983).
Zenz, F. A., "Scale up Fluid Bed Reactors," *Hydrocarbon Proc.*, **61**, 155 (1982).

Manuscript received Sept. 27, 2001, and revision received Jan. 7, 2002.